nature reviews materials

https://doi.org/10.1038/s41578-023-00618-1

Review article

Check for updates

Advantages, challenges and molecular design of different material types used in organic solar cells

Jicheng Yi [1,2,3], Guangye Zhang [1,3] ✉, Han Yu [2,3] & He Yan [2] ✉

Abstract

The performance of organic solar cells (OSCs) has increased substantially over the past 10 years, owing to the development of various high-performance organic electron–acceptor and electron–donor materials, including polymers, small molecules and fullerenes, used in the photoactive layer. Depending on the combination of donor and acceptor materials, OSCs can be categorized into several types: polymer–fullerene, polymer–small molecule, all-polymer and all-small molecule, as well as multicomponent OSCs in which the photoactive layer comprises three or more photoactive components. This Review provides an overview of the historical development of the different material types used in the photoactive layer of solution-processed OSCs and compares their advantages and limitations. Effective molecular design strategies for each type of OSC are discussed and promising research directions highlighted, particularly those relevant to facilitating the industrial manufacturing of OSCs.

Sections

[1]College of New Materials and New Energies, Shenzhen Technology University, Shenzhen, China. [2]Department of Chemistry and Hong Kong Branch of Chinese National Engineering Research Center for Tissue Restoration and Reconstruction, The Hong Kong University of Science and Technology, Clear Water Bay, Hong Kong, China. [3]These authors contributed equally: Jicheng Yi, Guangye Zhang, Han Yu. ✉e-mail: zhangguangye@sztu.edu.cn; hyan@ust.hk

Introduction

Solar cells are an important renewable energy technology owing to the abundant, clean and renewable nature of solar energy. The conventional silicon solar cell market has grown to reach a total annual installed capacity of 1.2 TW (ref. 1) and market sales totalling US$90 billion by 2022 (ref. 2). However, silicon-based photovoltaic cells have some drawbacks, including high-energy consumption during their fabrication[3–6], a long energy payback time[7,8] and the bulky, heavy nature of silicon panels[9,10]. Scientists and engineers are therefore working to develop alternative photovoltaic technologies, such as organic solar cells (OSCs) and perovskite solar cells, which can be produced using solution-coating processes at low temperatures. An advantage of these emergent photovoltaic technologies is that their production is much less energy-intensive than that of conventional silicon photovoltaics: the estimated energy consumption per watt is 0.26 kWh for silicon photovoltaics[11] but only about 0.02–0.07 kWh for OSCs[11,12]. Thus, these alternative PV technologies could reduce the carbon footprint of the photovoltaic industry. Furthermore, OSCs and perovskite photovoltaics can be fabricated into lightweight and flexible panels, making them suitable for installation in areas where conventional silicon photovoltaics are not practical[13–17], and OSCs do not contain toxic elements. These features make OSCs safe to deploy in modern cities where electricity consumption is high and rooftop space is limited.

Another important application area of organic photovoltaics (OPVs) is for indoor devices (note that when used indoors, OSCs should be referred to as OPVs). The rapid development of the internet of things is leading to an increase in the number of indoor electronic devices[18,19], which require a suitable energy source. One option is to install photovoltaic panels on these devices to convert indoor light into electricity, eliminating the need for disposable batteries[20–23]. Conventional silicon photovoltaics are not suitable for such applications because their absorption spectra do not match that of indoor light. However, the absorption spectra of the photoactive layer in OPVs can be readily tuned to match that of indoor lighting; this enables the power conversion efficiency (PCE) of OPVs under indoor conditions to reach beyond 30%[24–28], which is higher than that of silicon photovoltaics (~6%)[29]. In terms of stability, OPV devices have not yet achieved the desired level of stability for outdoor applications, such as operation under 1-sun intensity and high temperatures of up to 80 °C, which are typical stability testing conditions used in industry. However, their stability is probably sufficient for applications in more benign indoor environments. Furthermore, it is expected that OPV panels can sell at a higher price per unit area for internet of things applications than for applications in the outdoor power-generation market. Therefore, indoor applications will probably be the first economically viable market for OPV technologies.

The operation mechanism of OSCs is different from that of conventional silicon and emerging perovskite photovoltaics. In inorganic or perovskite materials, the photogenerated charges are generally easy to separate. However, in organic materials, photon absorption leads to partially bounded excited states called excitons that do not spontaneously separate into free charges. Instead, the excitons only separate into free charges at the interface of the electron–donor and electron–acceptor materials. Therefore, to maximize the contact interface essential for charge separation, the photoactive layer of OSCs (Fig. 1a) comprises a blend of donor and acceptor materials to form a bulk heterojunction (BHJ). As the choice of materials influences the device performance, the selection of the optimal material combination is crucial for achieving high PCEs in OSCs.

In the early days of OSCs, the photoactive layers were based on a polymeric donor and a fullerene acceptor. Following extensive materials development, there are now numerous alternatives for both the donor and acceptor materials. Besides polymer donors, small-molecule donors (SMDs) can also be used. For the acceptor, both small-molecule acceptors (SMAs) and polymeric non-fullerene acceptors (NFAs) have been developed. The introduction of these materials has led to several categories of solution-processable OSC depending on the composition of the photoactive layer, including polymer–fullerene, polymer–small molecule, polymer–polymer (all-polymer) and small molecule–small molecule (all-small molecule). Furthermore, the photoactive layer can comprise more than two photoactive components, in what is referred to as a multicomponent-active-layer device. Each of these categories of OSC has its own advantages and drawbacks. In this Review, we summarize the state-of-the-art developments for each of these OSC categories (Fig. 2) and compare their advantageous features and potential challenges. We also discuss molecular design strategies and touch upon key considerations that are important for the industrial production of OSC devices. Our aim is to inspire the OSC research community to develop OSC materials and/or device types that maximize the advantages of different donor and acceptor materials while minimizing or overcoming the existing problems.

Polymer–fullerene solar cells

Historically, fullerene derivatives such as [6,6]-phenyl-C_{61}-butyric acid methyl ester ($PC_{61}BM$) have been the most used acceptors in OSCs. The BHJ concept was introduced in 1995 by Heeger and co-workers, who blended a poly(*p*-phenylene vinylene) (PPV)-based polymer donor MEH-PPV (Supplementary Fig. 1) with $PC_{61}BM$[30], with a similar concept independently reported by Friend and co-workers in the same year[31]. In the report of MEH-PPV–$PC_{61}BM$ OSCs[30], ultrafast electron transfer was observed from the polymer donor to the $PC_{61}BM$ acceptor (Fig. 2), laying the groundwork for further development of BHJ OSCs.

There are several reasons why fullerene derivatives, with $PC_{61}BM$ as the most representative example, are popular acceptors for OSCs. First, $PC_{61}BM$ is a natural and high-performance electron-transport semiconductor that has a higher electron mobility than that of many other electron-transporting organic semiconductors[32]. Most electron-transporting polymeric semiconductors have an electron mobility on the order of 10^{-5}–10^{-6} $cm^2\ V^{-1}\ s^{-1}$, whereas $PC_{61}BM$ exhibits an electron mobility of about 10^{-2}–10^{-3} $cm^2\ V^{-1}\ s^{-1}$ (measured using the space-charge-limited current method). Second, owing to the spherical molecular shape of fullerenes, they can form a 3D charge-transport network in the BHJ structure. Third, a prerequisite to efficient OSCs is the formation of reasonably small donor and acceptor domains with sizes in the range 20–30 nm. Fullerene acceptors can form acceptor phases with this domain size owing to the relatively amorphous nature of the material. By contrast, other high-performance electron-transporting polymeric semiconductors have high crystallinity and form large domains in BHJ blends[33,34]. Overall, $PC_{61}BM$-type fullerene acceptors offer reasonably high electron mobility and suitable domain sizes for the operation of BHJ OSCs. Thus, the early development of OSC materials was mostly focused on polymer donors[32] (Fig. 2).

First-generation donor materials are PPV-based polymers that have a large bandgap of 2.5 eV and limited hole mobility[31]. Poly(3-hexylthiophene) (P3HT)-based (Supplementary Fig. 1) hole-transporting organic semiconductors were subsequently introduced, leading to an increase in the fill factor and efficiency of OSCs[35], but the absorption range of P3HT polymers is narrow owing to their

large optical bandgap. The next generation of polymer donors was based on low-bandgap polymeric semiconductors, such as PCPDTBT[36] (Supplementary Fig. 1) and PTB7 (ref. 37) (Fig. 1b); these materials are copolymers that contain electron-rich and electron-deficient units (often referred to as donor (D) and acceptor (A) units, respectively), which can effectively lower the bandgap, leading to an increase in the absorption and efficiency of OSC devices. With PTB7, the PCE of polymer–fullerene OSCs increased from 4% to 7.4%[37]. In terms of stability, PTB7-Th:[6,6]-phenyl-C_{71}-butyric acid methyl ester ($PC_{71}BM$) solar cells can retain >92% of their initial PCE under continuous ultraviolet (UV)-filtered 1-sun illumination up to 2,300 h (with an extrapolated T_{80} of 14,250 h, in which T_{80} is the time for the PCE to decrease by 20%), which is the longest T_{80} lifetime reported for a polymer–fullerene OSC under these conditions[38] (the stability test conditions are summarized in Supplementary Table 1). However, the charge-transport ability of these low-bandgap donor polymers is limited by their low crystallinity. A long-existing dilemma in the design of polymer donors is that highly crystalline hole-transporting semiconductors often form excessively large domains, whereas the hole-transporting ability of amorphous polymers is too low. This dilemma was partially solved with the development of a series of polymer donors that form highly crystalline yet reasonably small polymer domains[39–41], enabled by the temperature-dependent aggregation behaviour of the polymers, which allows for control of the domain morphology. Using these polymer donors, thick-film polymer–fullerene devices were fabricated with fill factors of 74% and PCEs near 11.7%[42] (Table 1). However, owing to the poor absorption of fullerenes and large voltage loss (V_{loss}) from the optical bandgap (E_g) to the open-circuit voltage (V_{OC}) ($V_{loss} = E_g - V_{OC}$) of the solar cell, the PCE of polymer–fullerene devices is still limited at about 12%[43–46].

Advantages and challenges

The most important advantage of fullerene acceptors is their relatively high electron mobility (Table 2), typically estimated in the range 10^{-2}–10^{-3} $cm^2\ V^{-1}\ s^{-1}$ (refs. 47,48), compared with that of other types of acceptor materials. The high electron mobility allows for the fabrication of thick-film (300-nm) OSC devices with high efficiencies[49,50], thus making fullerene-based films amenable to large-scale roll-to-roll industrial production[51]. In addition, fullerene-based OSCs can achieve good performance using the inverted OSC architecture, which is the device structure commonly used for OSC production in industry. Over the past 15 years, there has been extensive research and development efforts in the OSC industry focusing on the production and optimization of fullerene-based OSCs. As a result, the OSC industry has developed mature production processes, device architectures and supplementary materials (such as interlayers) for inverted-structure fullerene-based OSC devices[52]. Thus, this category of OSC is still the only one to have made notable progress in terms of industrial production.

The major disadvantage of fullerene-based OSC devices is the large voltage loss. For the highest-efficiency fullerene-based OSCs, the voltage loss is in the range 0.8–0.9 eV (ref. 42), which has restricted the PCE of fullerene OSCs to about 12%. The absorption window of fullerene acceptors is also relatively narrow (about 300 nm) compared with that of polymer donors and most NFAs. Furthermore, it is quite challenging to tune the energy levels and chemical structures of fullerene derivatives[53,54], so that the choice of fullerene acceptors is more limited compared with the extensive libraries of small-molecule or polymer acceptors (discussed in a subsequent section). Owing to these limitations, the materials development and efficiency improvement of polymer–fullerene-based binary OSCs appear to have reached an end, driving the OSC research community towards non-fullerene OSCs in the past few years.

Polymer–small-molecule solar cells

To overcome the limitations of fullerene acceptors, non-fullerene SMAs are being explored as possible replacements. The development of SMAs for OSCs has also been facilitated by rapid advances in the development of electron-transporting organic semiconductors for organic field-effect transistors (OFETs) since 2004 (ref. 55). Historically, it has been much more challenging to achieve high-mobility electron-transporting organic semiconductors than hole-transporting ones for either OSC or OFET applications. The success in developing a perylene diimide (PDI)-based high-performance small-molecule electron-transporting organic semiconductor in 2004 was not only a breakthrough for OFETs but also provided inspiration for the design of SMAs for OSCs.

Molecular design of small-molecule acceptors

PDI-based electron-transporting organic semiconductors, such as SF-PDI2 (ref. 56) (Supplementary Fig. 2), were one of the most popular classes of first-generation SMAs. The PDI unit was selected because of its high electron mobility, as demonstrated in OFET applications, and its deep lowest unoccupied molecular orbital (LUMO) level, which can match with the relevant energy levels of polymer donors[57–60]. However, a major problem with PDI-based acceptors is their tendency to aggregate owing to their large co-planar aromatic structure and high crystallinity, resulting in excessively large domains in BHJ blends[61]. To mitigate this problem, PDI dimers or trimers with twisted intramolecular structures were designed to reduce the strong aggregation and high crystallinity of the PDI units[62,63]. This approach indeed reduces the acceptor domain size in the BHJ blend but, unavoidably, the decrease in crystallinity also decreases the charge mobility of the PDI acceptors. This dilemma is similar to that faced in the design and development of polymer donors.

In 2015, a major breakthrough in SMAs was achieved when Zhan and co-workers reported a class of NFAs based on ITIC[64] (Figs. 1b and 2). ITIC consists of a core structure comprising seven fused aromatic rings, capped at either end by a rigid electron-withdrawing end group, with four alkylphenyl side chains appended to the sp^3-hybridized carbon bridges of the core. Compared with earlier PDI-based non-fullerene OSCs, ITIC-based OSCs achieved markedly improved device performance[65–69], which can be attributed to the molecular features of ITIC. The rigidity of ITIC-type molecules enables them to form crystalline acceptor domains with reasonably high electron mobility; however, the four alkylphenyl side chains prevent excessive aggregation. Moreover, ITIC has an A–D–A-type structure in which the donor unit is protected by bulky alkylphenyl side chains, whereas the acceptor units are fully exposed co-planar aromatic structures that can participate in π–π stacking to form an efficient electron-transport network. ITIC-based acceptors can therefore achieve more efficient electron transport than PDI oligomers while maintaining a reasonably small domain size[64,70]. This balance between high crystallinity and small acceptor domain size was challenging to achieve for conventional PDI-based acceptors and is one of the most important factors contributing to the success of state-of-the-art SMAs, including ITIC and Y6-type SMAs (discussed in a subsequent section).

The choice of polymer donor is also crucial for achieving high-efficiency non-fullerene OSCs. Not long after ITIC molecules were

a

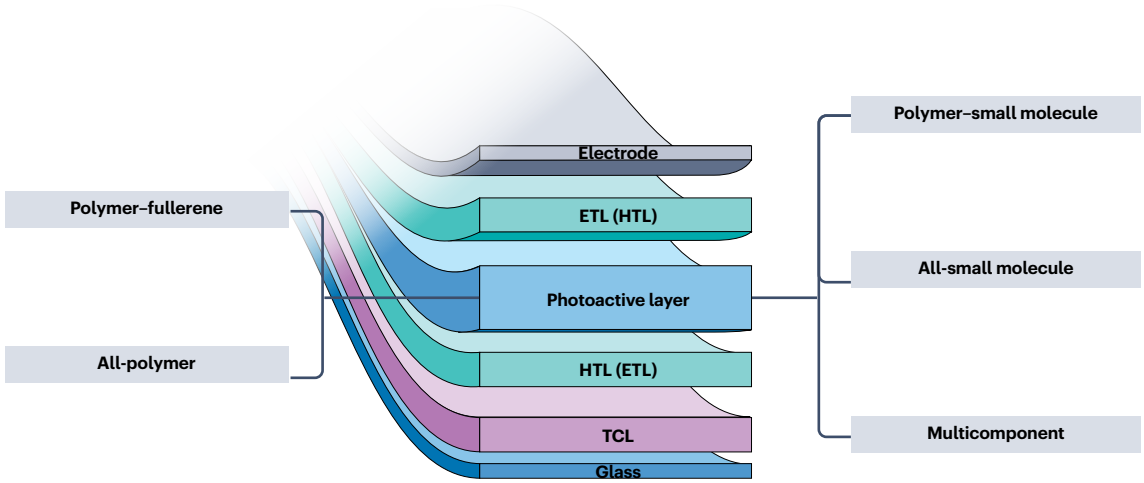

b

PTB7
R = 2-ethylhexyl

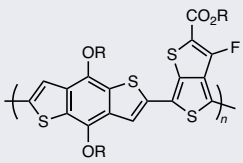

PffBT4T-2OD

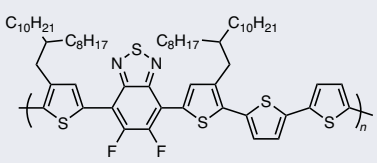

BTR

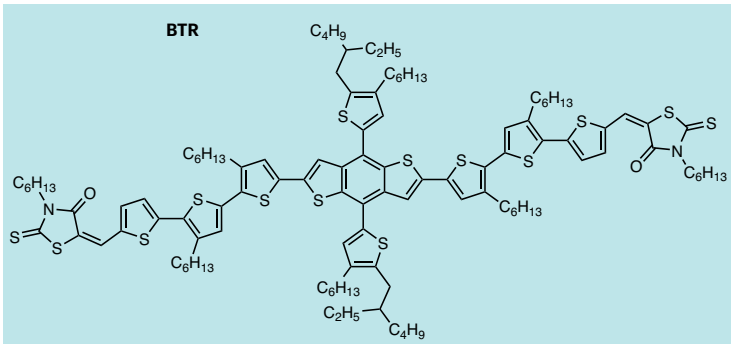

PBDB-T: R = H, **PM6:** R =F

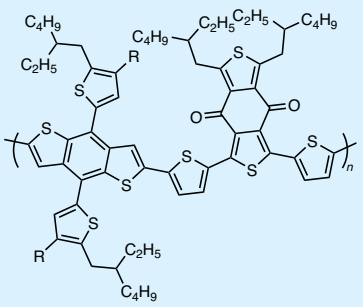

ITIC

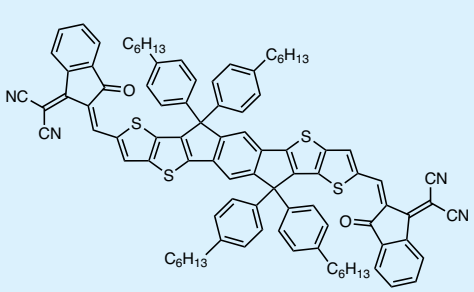

Y6

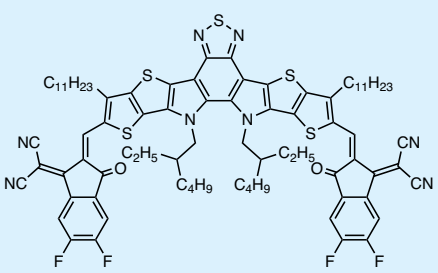

N2200

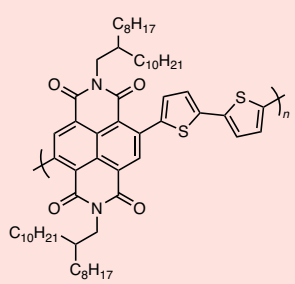

PZ1

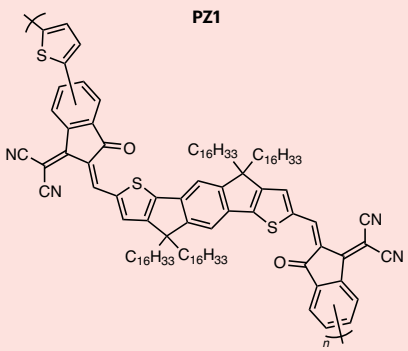

PY-IT

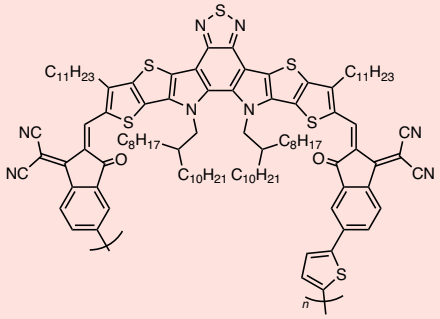

Fig. 1 | Typical organic solar cell device structure and representative photoactive materials used in organic solar cells. a, A typical organic solar cell (OSC) comprises an electron-transport later (ETL), hole-transport layer (HTL), transparent conducting layer (TCL) and a photoactive layer. The photoactive layer is composed of a blend of acceptor and donor materials, which form a bulk heterojunction. Depending on the combination of acceptor and donor materials, there are five main categories of OSC: polymer–fullerene, polymer–small molecule, all-polymer, all-small molecule and multicomponent. **b**, Chemical structures of some representative materials used in the photoactive layer of different types of OSCs. The colour indicates the main category of OSC that the material is used in: polymer–fullerene (grey), polymer–small molecule (dark blue), all-polymer (pink) and all-small molecule (light blue). BTR, benzo-dithiophene terthiophene rhodamine.

reported in 2015, polymer donors that exhibit temperature-dependent aggregation were shown to achieve highly efficient non-fullerene OSCs, even when paired with conventional PDI-based acceptors[71,72]. Although these polymer donors were initially developed for fullerene-based acceptors, structural changes (such as alkyl chain modifications), and thus tuning of the polymer properties, enabled their application in non-fullerene OSCs[73]. Along with the emergence of SMAs, high-performance polymer donors were also developed, including PffBT4T-2OD[39] (Fig. 1b), and two extremely important polymer donors that have become widely used named PBDB-T[74] (Fig. 1b) and PM6 (ref. 75) (Figs. 1b and 2). The temperature-dependent UV–Vis absorption spectra of these polymer donors revealed that they exhibit blueshifted absorption in solution at high temperature. When the solution temperature dropped from 80 °C to 25 °C, the absorption exhibited a drastic bathochromic shift with a shoulder peak appearing at about 700 nm, indicating the aggregation of the polymers in solution[39]. Polymer donors with this temperature-dependent aggregation can achieve moderately high charge mobility while forming small donor domain sizes[73]; this forms the basis of a reasonably good BHJ morphology and allowed for the rapid subsequent development of various SMAs.

The next major breakthrough in the development of non-fullerene OSCs was the design of a family of SMAs represented by the prototypical example named Y6 (ref. 76) (Figs. 1b and 2). Y6-type SMAs can achieve much increased device efficiency compared with that of ITIC-based devices and have pushed the PCE of OSCs to beyond 19% in the past 3 years[77–81]. Comparing the structures of Y6 and ITIC-type SMAs, there are three main differences. First, the central part of Y6 contains an electron-deficient benzothiadiazole unit that endows Y6 with an A–D–A′–D–A structure, in contrast to the A–D–A structure of ITIC. Second, whereas ITIC has central symmetry, Y6 has mirror symmetry with a 'banana-like' molecular shape. This difference in molecular shape and symmetry could change the crystal structure as well as aggregation and molecular-packing properties of the molecules[82–85]. Finally, whereas the alkyl chains on ITIC are positioned at the two sp^3-hybridized carbon bridges, the central alkyl chains on Y6 are appended to the nitrogen atoms of the pyrrole units. As the alkyl chains on ITIC are essentially pointing out of the plane of the aromatic backbone, whereas the alkyl chains on Y6 could be coplanar with the molecular backbone, the alkyl chains on ITIC might be less conducive to the molecular packing of the acceptor molecule than those on Y6. These structural differences result in an improvement of various device parameters. For example, the voltage loss of Y6-based non-fullerene OSCs is much smaller than that of ITIC-based devices. The best-performing Y6-based non-fullerene OSCs have a bandgap of 1.38 eV and a V_{OC} of 0.87 V, leading to a voltage loss as small as 0.5 eV (ref. 86). By contrast, for the ITIC family, the best-performing device has a voltage loss of 0.6 eV (ref. 87). Various factors could contribute to the reduced voltage loss of Y6-based OSCs, including the decreased non-radiative recombination loss of Y6-based devices[88–91].

Following the report of Y6-type acceptors, notable research efforts were directed towards the design of non-fullerene SMAs similar to Y6, involving the modification of the central core, side chains and end groups. Alternatives to the electron-deficient benzothiadiazole core include benzotriazole[92], benzoquinoxaline[93] and benzoselenadiazole cores[94]. Modification of the core can change the energy of the frontier orbitals of the molecule and upshift the highest occupied molecular orbital (HOMO) and LUMO, resulting in an increase in the V_{OC} and potentially a decrease in the voltage losses of the final OSCs. The second-position branched alkyl chains appended to the nitrogen atoms of the pyrrole units in the parent Y6 molecule have been replaced with third-position or fourth-position branched alkyl chains[95], which can reduce the steric hindrance and increase the crystallinity of the NFAs. Moreover, attaching much longer alkyl chains at these nitrogen positions can improve the processibility of OSCs over large areas using non-halogenated solvents, which is another important research direction for OSCs[96]. The alkyl chain at the β-positions of the outer thiophene units can also be modified. These alkyl chains have two functions: first, they ensure the formation of the *trans*-diene conformation between the thiophene unit and bridge double bond and thus rigidify the geometry and molecular shape of Y6 and, second, they alter the crystallization behaviour and molecular-packing mode. Replacement of the straight alkyl chain at the β position of the thiophene unit with a second-position branched 2-butyloctyl (2-BO) alkyl chain[85], although seemingly a minor modification, resulted in surprisingly large changes in the absorption of the molecule and the V_{OC} of the final OSC. The resulting molecule, L8-BO (Fig. 2 and Supplementary Fig. 2), exhibits a more condensed molecular assembly with additional π–π packing motifs (thus providing more charge-hopping channels) than Y6, based on single-crystal and grazing-incidence wide-angle X-ray scattering analysis, leading to an exceptionally high fill factor (81.5%) in the final OSC device. To date, the polymer–small-molecule OSCs with the highest efficiencies are those fabricated through the sequential deposition of the D18 donor (Supplementary Fig. 2) and the L8-BO acceptor[97] (Table 1). Besides changes in the branching, the alkyl chain has been replaced with alkylphenyl[98,99], alkylthiophene[100,101] and alkoxy side chains[102]. The alkoxy side chain effected the greatest change to the energy levels of the molecule by upshifting the HOMO and LUMO. By contrast, despite having no effect on the energy levels, the alkylphenyl and alkylthiophene side chains had a substantial effect on the intermolecular interactions, π–π stacking distance and phase separation of the molecule as well as the blends with a donor material. As a result of the change in crystal packing, an OSC with a PCE of more than 18% was achieved using the acceptors with the alkylphenyl or alkylthiophene side chains. Finally, the end group of Y6, 2-(5,6-difluoro-3-oxo-2,3-dihydro-1H-inden-1-ylidene)malononitrile (IC-2F), has been replaced with numerous other end groups, including those with either stronger or weaker electron-withdrawing ability, thus downshifting or upshifting the energy levels of the SMAs, respectively[103,104]. Furthermore, Y6 derivatives with two different end groups can exhibit special

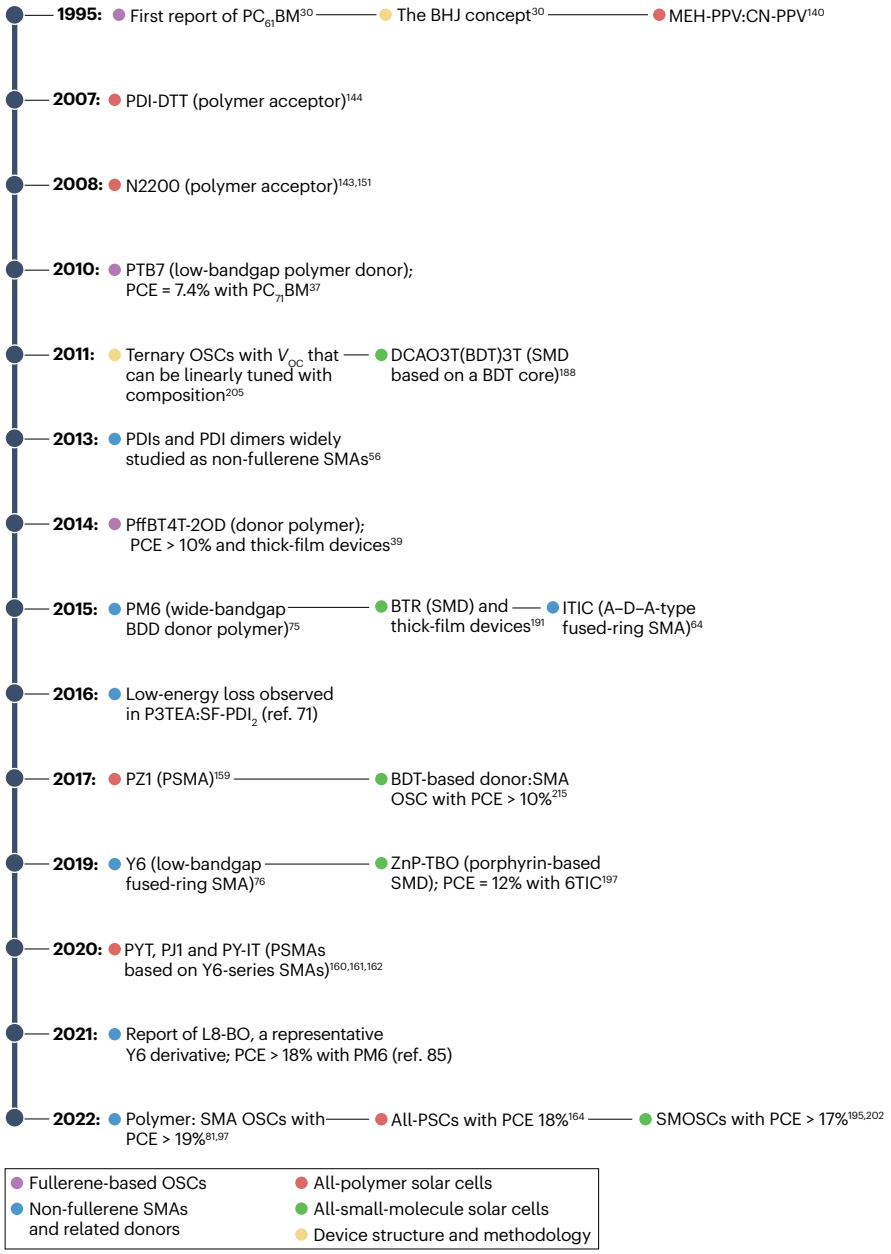

Fig. 2 | Timeline of the development of organic solar cell materials. Milestones in different areas of organic solar cell (OSC) development[30,37,39,56,64,71,75,76,81,85,97,140,143,144,151,159–162,164,188,191,195,197,202,205,215]. All-PSC, all-polymer solar cell; all-SMOSC, all-small-molecule OSC; BDD, benzo[1,2-c:4,5-c′]-dithiophene-4,8-dione; BDT, benzo-[1,2-*b*:4,5-*b*′] dithiophene; BHJ, bulk heterojunction; BTR, benzodithiophene terthiophene rhodamine; CN-PPV, cyano-poly(*p*-phenylene vinylene); DTT, dithienothiophene; MEH-PPV, poly(2-methoxy-5-(2′-ethyl-hexyloxy)-1,4-phenylene vinylene); N2200, poly{[N,N′-bis(2-octyldodecyl)-naphthalene-1,4,5,8-bis(dicarboximide)-2,6-diyl]-alt-5,5′-(2,2′-bithiophene)}; $PC_{61}BM$, [6,6]-phenyl-C_{61}-butyric acid methyl ester; $PC_{71}BM$, [6,6]-phenyl-C_{71}-butyric acid methyl ester; PCE, power conversion efficiency; PDI, perylene diimide; PffBT4T-2OD, poly[(5,6-difluoro-2,1,3-benzothiadiazol-4,7-diyl)-alt-(3,3‴-di(2-octyldodecyl)-2,2′;5′,2″;5″,2‴-quaterthiophen-5,5‴-diyl)]; PSMA, polymerized SMA; SMA, small-molecule acceptor; SMD, small-molecule donor; V_{OC}, open-circuit voltage.

functions. For example, one end group can act as a building block to stabilize the film morphology, whereas the other can form a desirable stacking for efficient electron transport, thus increasing the PCE and stability of OSCs[105–109].

Despite their excellent performance, state-of-the-art SMAs are typically fused-ring aromatic molecules that are complicated to synthesize, which increases the cost of the material and thus the OSC panels. To reduce the cost of the acceptor material, non-fused-ring acceptors have been developed (we refer readers to other reviews for more details[110,111]). Generally, non-fused-ring SMAs are much easier to synthesize, which increases the overall synthetic yields and thus substantially reduces the cost of the material[112,113]. The disadvantage of non-fused-ring SMAs is that the aromatic backbone is connected using carbon–carbon single bonds, which could introduce some conformational twisting, thus affecting the coplanarity and π–π stacking of the molecule[114–118]. This weakness can be partially solved by introducing intramolecular non-covalent bonds as a form of conformational locking[119,120]. With such strategies, the performance of non-fused-ring SMAs has increased over the past 2–3 years to achieve a PCE of up to 16.2%[121].

Advantages and challenges

The most important advantage of SMA-based OSCs is their high device efficiencies enabled by the small voltage loss (Table 2). The voltage loss for the highest-efficiency SMA-based OSC is as low as 0.54 eV (ref. 97), compared with 0.85 eV for devices with fullerene-based acceptors[42].

The reduction in voltage loss is due to the reduced gap between the HOMO levels of the donor and acceptor materials and a decrease in the non-radiative recombination loss, as evidenced by the higher electroluminescence external quantum efficiency (EQE_{EL}). Potentially, this voltage loss can be further decreased to 0.45 eV (refs. 92,122,123) with a further reduction of the non-radiative recombination loss. In principle, this decrease in the voltage loss could enable the realization of OSCs with PCEs of more than 21%[124].

The second advantage of SMA OSCs is their rapid development pace. In the SMA OSC community, most research efforts have been focused on device optimization with newly designed Y6-type SMAs and an existing high-performance polymer donor. As the combination of a polymer donor and a Y6-type SMA has a good chance of forming a nearly optimal OSC morphology, polymer–SMA devices based on Y6-type SMAs have a good probability of achieving high efficiencies. Also, as the design and synthesis of Y6-type SMAs are relatively simple and fast, more than 1,000 SMAs that enable high-efficiency devices have been developed within 2–3 years. By contrast, for fullerene-containing OSCs, the material development pace had been slower because of the much greater time and effort required to develop a high-performance polymer donor.

The main challenge for SMA-based OSCs is their device stability. Although some SMA OSCs, such as IDTBR-based systems, can achieve long stability (Supplementary Table 1), the device PCE of these stable OSCs is relatively low (<10%)[125–128]. By contrast, current high-efficiency SMA OSCs suffer from relatively poor device stability (Supplementary Table 1), especially in inverted devices with poly(3,4-ethylenedioxythiophene):poly(styrene sulfonate) (PEDOT:PSS) as an interlayer, which is currently used by industry[129,130]. The unsatisfactory stability of current-generation SMAs could be due to numerous factors, including the double bond linking the core and the end group of typical SMAs. The vinylic hydrogen is particularly acidic and is the cause of photochemical degradation upon long-term device operation. Considerable research efforts have been devoted to solving this problem by changing the motif containing the carbon–carbon double bond that links the D–A units to other chemical moieties[131,132] (IDTT-CT; Supplementary Fig. 6); some initial studies have shown promising improvements in device stability, but the device efficiencies are sacrificed in most cases.

Another challenge of current SMA OSCs is that the devices with the highest efficiencies are typically fabricated using processing conditions that cannot be adopted in industry. The OSC industry currently has the following requirements for large-scale OSC production: processing under ambient conditions, use of non-halogenated solvents, inverted OSC device structures and use of PEDOT-based conducting polymers as the top charge-extraction layer. Although SMA OSCs can achieve PCEs of 18–19%, most of these devices were fabricated under an anhydrous nitrogen atmosphere using chloroform as solvent and with a regular device structure. If the current high-efficiency SMA materials were to be used to fabricate OSCs using industrial processes, the device PCE could be reduced to <10% owing to the incompatibility of these SMA materials with industrial fabrication processes[133]. Although most polymer–SMA OSCs reported have the regular device structure, an extrapolated T_{80} lifetime of >11,000 h was achieved for a PBDB-T:ITIC-2F-based device with an inverted configuration[134,135] (Supplementary Fig. 2 and Supplementary Table 1). Moreover, a PM6:Y6-based inverted device with an Ir/IrO_x electron-transporting layer achieved a lifetime of >10,000 h (ref. 136). These efforts in investigating inverted structures are very important and should be encouraged, as this work helps to bridge the gap between academic research and industry adoption. However, the hole-transport layer used in these works was vapour-deposited MoO_3, not a solution-processed conducting polymer (such as PEDOT:PSS) preferred by industry.

The limited number of reports on PEDOT:PSS-based OSCs is also partially due to the intrinsic material drawbacks of PEDOT:PSS. For example, the acidity of PEDOT:PSS and the aqueous nature of its formulations can cause damage to the photoactive layer and thus degradation of OSC devices[137]. In addition, the wettability of PEDOT:PSS aqueous solutions on the photoactive layer is quite poor, leading to severe de-wetting or other film coverage issues. It is important to solve these issues to develop fully printed (from bottom electrode to top electrode) OSCs with good long-term stability. To this end, an alcohol-dispersed formulation has been demonstrated to address the aforementioned problems of PEDOT:PSS[138,139]. This approach increased the stability of a Y6-based fully printable device with an inverted structure (Ag nanowires/polyethyleneimine-Zn/PM6:PC_{71}BM:Y6/PEDOT:F/Ag nanowires). The device retained 83% of its initial PCE of 15% after 1,330 h of light soaking — an impressive performance that suggests this approach could help to facilitate the industrial fabrication of OSCs.

All-polymer solar cells

All-polymer solar cells (all-PSCs) are OSCs in which both the donor and acceptor components are polymers. In one of the first examples of BHJ OSCs, reported in 1995, two polymers, MEH-PPV and CN-PPV (Supplementary Fig. 1), were used to construct the photoactive layer[140]. It was initially thought that it might be easier for two polymers to form an interpenetrating and bi-continuous donor–acceptor network than for a polymer–small molecule combination, as polymers have the advantage of forming a continuous charge-transporting network even at a low weight ratio in a blend. Also, it is reasonable to expect that all-PSCs should have better thermal and morphological stability and improved

Table 1 | Single-junction binary-active-layer organic solar cells with the highest power conversion efficiencies (as of January 2023)

Photoactive layer	Materials	V_{OC} (V)	J_{SC} (J_{EQE}) (mA cm^{-2})	FF (%)	PCE (%)	Certified PCE (%)	Active area (mm^2)	Masked measurement?	Ref.
Polymer–fullerene	PffBT4T-C_9C_{13}:PC_{71}BM	0.788	20.2 (19.9)	74	11.7	11.48±0.25	5.9	Yes	42
Polymer–SMA	D18:L8-BO	0.918	26.86 (26.63)	77.25	19.05	18.9	3.169	Yes	97
All-polymer	PQB-2:PY-IT	0.942	24.2 (23.7)	79.5	18.1	17.6	6.169	Yes	164
All-small molecule	TB-F:L8-BO	0.87	25.41 (24.77)	76.7	17.0	NA	4.3	NA	195

FF, fill factor; J_{EQE}, integrated J_{SC} calculated from external quantum efficiency (EQE) spectra; J_{SC}, short-circuit current density; NA, not available; PCE, power conversion efficiency; SMA, small-molecule acceptor; V_{OC}, open-circuit voltage.

Table 2 | Advantages and challenges of the different types of organic solar cells

Subcategory	Advantages	Challenges	Key molecular design strategies
Polymer–fullerene	High electron mobility; thick-film devices, important for large-scale roll-to-roll production; compatible with the inverted OSC architecture used in industrial OSC production	Large voltage loss; poor absorption; low device efficiencies; difficult to tune the energy levels and chemical structures of fullerenes	Design donor polymers with a strong temperature-dependent aggregation property
Polymer–small molecule	High device efficiencies enabled by small voltage loss; rapid development owing to good morphology control of blends and ease of the design and synthesis of SMAs	Relatively low device stability; limited progress towards industrial production	A–D–A-type SMAs with rigid backbones, as in ITIC and Y6; banana-shaped SMAs, such as Y6
All-polymer	Good thermal stability and photostability; excellent mechanical properties for the fabrication of stretchable and flexible devices; high device efficiencies	Batch-to-batch variation of molecular weight; challenging morphology control; lower electron mobility than that of SMAs	Design polymer acceptor based on high-performance SMAs — the so-called polymerized SMA strategy
All-small molecule	Good batch-to-batch reproducibility	Challenging morphology control; low viscosity of active-layer solution, thus difficult to be produced industrially; stability remains to be investigated	Engineering of core, side chain and end groups of SMDs and SMAs
Multicomponent	Wide absorption range; fine-tuning of energy levels by adjusting the composition of the organic alloy; possible to tune the crystallinity, domain size and morphology of BHJ blends	Complicated morphology	One donor polymer combined with two SMAs that form organic alloys; one donor polymer combined with one SMA and a small amount of a fullerene acceptor

BHJ, bulk heterojunction; OSC, organic solar cell; SMA, small-molecule acceptor; SMD, small-molecule donor.

mechanical properties[141,142], such as higher tensile and flexural toughness. However, the development of all-PSCs was extremely slow before 2009, limited by the acceptor material and, specifically, the lack of high-performance electron-transporting polymeric semiconductors. The report of a high-mobility electron-transporting polymeric semiconductor in the OFET field in 2009 inspired the development of the next generation of all-PSCs[143].

Molecular design of polymer acceptors

One of the reasons for the poor performance of early-generation MEH-PPV:CN-PPV-based all-PSCs was the poor electron mobility of the acceptor CN-PPV. Since 2007, researchers in the OSC field have been applying their experience in preparing high-performance hole-transporting polymers using the electron push–pull effect to the design of electron-transporting polymers. Among these electron-transporting polymers, D–A copolymers based on naphthalenediimide (NDI) and PDI units have substantially higher electron mobility (10^{-3}–10^{1} cm^2 V^{-1} s^{-1} in organic thin-film transistor devices) than do PPVs[142–148]. For example, a PDI-based polymer acceptor, PDI-DTT (Supplementary Fig. 3), reported in 2007 (ref. 144) showed an OFET electron mobility of 1.3×10^{-2} cm^2 V^{-1} s^{-1}. When used in combination with a bi(thienylenevinylene)-substituted polythiophene polymer donor, the all-PSC device demonstrated a PCE of >1%. More importantly, PDI-DTT showed strong (with a peak absorption coefficient of about 10^5 cm^{-1}) and broad absorption in the visible region (it is an almost black solid), indicating the potential of such materials for replacing fullerenes. This work led to the development of PDI-based polymer acceptors such as PDI-V[149] and NDP-V[150] (Supplementary Fig. 3) in the following years.

Another milestone in the development of electron-transporting polymers was the report of N2200 (refs. 143,151) (Figs. 1b and 2) in 2008, which has continued to attract attention in the organic electronics community owing to its high electron mobility. From 2011, this NDI derivative was used as an electron acceptor to fabricate all-PSCs, with the PCE of N2200-based all-PSCs increasing from 1%[152] to 11.76%[153]. The increase in the PCE is attributable to the optimization of the polymer itself, such as tuning the molecular weight, but also to the knowledge gained by the field in other aspects, including morphology regulation[152], the design of compatible donors[154] and device engineering. N2200 is still a popular choice to construct all-polymer ternary blends. In addition to PDI and NDI, other electron-deficient building blocks used to design polymer acceptors include bithiophene imides, isoindigos, thieno[3,4-*c*]pyrrole-4,6-diones, arenes incorporating a B ← N coordination bond, cyano-functionalized arenes and diketopyrrolopyrroles[155]. Among these, a B ← N-containing copolymer[156], PBN-12 (Supplementary Fig. 3) and polymer acceptors based on cyano-functionalized arenes, such as DCNBT-IDT[157] and DCNBT-TPIC[158] (Supplementary Fig. 3), led to all-PSCs with PCEs of >10%.

The success of A–D–A-type ITIC SMAs inspired the idea of using the ITIC derivative IDIC (Supplementary Fig. 4) as the key building block to construct electron-transporting copolymers[159]. The use of IDIC as the key building block and thiophene as the π-linking unit led to the polymerized SMA (PSMA) named PZ1 (Figs. 1b and 2). PZ1 showed improved thermal stability than the corresponding SMA (IDIC-C16) (Supplementary Fig. 3), excellent absorption coefficients (>10^5 cm^{-1} at 700 nm), enhanced EQEs in the near-infrared region and a PCE of 9.19% in combination with the polymer donor PBDB-T in all-PSC devices. As the field of SMAs has been advancing rapidly, this result underlines the potential of the PSMA strategy to address problems of previous polymer acceptors, such as the low quantum efficiencies in the near-infrared region of N2200, and the production of polymer acceptors with easily tunable electronic properties.

From 2020 onwards, Y6 and its derivatives have been used to build more efficient PSMAs. For example, an A–DA′D–A-type SMA (Y5-C20) was used as the building block to obtain the PSMA PYT[160] (Supplementary Fig. 3). By adjusting the molecular weight of the PSMA, the morphology of the PM6:PYT photoactive layer could be tuned and the final all-PSC achieved a maximum PCE of 13.44%. A PSMA named PJ1 (Supplementary Fig. 3) was synthesized by copolymerizing the TTPBT-IC unit with thiophene; combined with PBDB-T in the photoactive layer,

the PBDB-T:PJ1-based all-PSC achieved a PCE of 14.4%[161]. A strategy to reduce the energetic disorder, and thus reduce the recombination loss and subsequently voltage loss, is to obtain regioregular polymers with isomerically pure end groups, as demonstrated with PY-IT (Fig. 1b), which showed good electron-transport properties and, in combination with PM6, enabled an all-PSC with a high PCE of 15.05%[162]. More recently, a polymer donor named PQM-Cl (Supplementary Fig. 3) has been designed that showed excellent compatibility with PY-IT, resulting in an all-PSC with a high PCE of 18%[163]. Later, the same group synthesized three random terpolymer donors, one of which, PQB-2 (Supplementary Fig. 3), afforded an all-PSC with a PCE of 18.1% when combined with PY-IT[164] (Table 1). In another example, two polymer acceptors (PY-SSe-V and PY-Cl) with different aggregation tendencies were synthesized and applied in a sequentially processed ternary all-PSC device with PM6 as the donor, achieving a PCE of 18.14%[165].

Advantages and challenges

The main advantage of all-PSCs is their improved stability compared with other categories of non-fullerene OSC (Table 2). As polymer acceptors are expected to exhibit better thermal stability than SMAs, efforts have been devoted to increasing the thermal stability of OSCs by incorporating polymer acceptors. Several research groups have reported impressive thermal stability for all-PSC devices. In one example, all-PSC devices retained 80% of their initial efficiency after thermal annealing at 85 °C for >6,000 h (ref. 166) (Supplementary Table 1). Comparison of the thermal stability of three different SMAs and their corresponding PSMAs demonstrated that the thermal stability can be greatly increased for the polymer acceptor, with, in the best case, >90% of the initial PCE retained after thermally annealing the device at 100 °C for more than a year[167] (Supplementary Table 1).

In terms of photostability, all-PSC devices have demonstrated much improved light-soaking stability. For example, PM6:PY2F-T:PYT-based ternary all-PSCs can maintain >90% of their initial PCE after 2,000 h of continuous light soaking, which can be extrapolated to a T_{80} lifetime of >20,000 h — the most impressive stability performance reported for an OSC to date[168] (Supplementary Table 1). Another expected advantage of all-PSCs is their outstanding mechanical properties for application in stretchable and flexible devices. In an early example, an all-PSC comprising PBDTTTPD as the polymer donor and P(NDI2HD-T) as the polymer acceptor achieved an elongation-at-break of 7.16%, a 26-fold increase over corresponding fullerene devices[169]. More recently, a device with excellent stretchability was reported in which a flexible spacer was used in the molecular design of the polymer acceptor. The all-PSC achieved a PCE of 10.6% as well as outstanding device stretchability (with a strain of 36.7% at 80% of the initial PCE)[170]. The excellent stability and mechanical properties of all-PSCs opens opportunities for applications such as wearable devices.

A major problem for all-PSCs is the challenge of controlling the molecular weight of both the polymer donor and acceptor and the resulting complicated morphologies formed by two polymers. Compared with small molecules, the properties of polymer materials depend on their molecular weight, which can vary greatly from batch to batch, and this issue is compounded in all-PSCs. For example, the most widely used high-performance polymer donor, D18, can vary in performance even with a slight variation in its molecular weight[171]. This variation poses challenges in the scale-up and production of polymer-based OSCs. To overcome these problems, researchers must either understand the relationship between the polymer molecular weight and properties or develop polymers whose performance is not sensitive to their molecular weight. The second disadvantage of polymer acceptors is that the electron mobility of polymer acceptors is lower than that of the SMAs. This inferiority is not completely unexpected, as polymer materials contain a mixture of molecules with different molecular weights, whereas SMAs are pure. Thus, SMAs can typically form more crystalline microstructures, enabling higher charge mobility, providing that other structural features are the same. This outcome is particularly true for the state-of-the-art Y6-based polymer acceptors and SMAs, which essentially have the same core structures, except for the number of repeat units. A direct comparison shows a clear reduction in the electron mobility of polymer acceptors compared with SMAs with the same core structure[172]. Furthermore, the morphology control in all-PSCs, including control of the vertical phase separation, is challenging owing to both materials having long chains. However, sequential processing has been shown to address this issue in a few all-PSC systems[173,174].

All-small-molecule solar cells

The main reason to develop all-small-molecule OSCs (all-SMOSCs) is to avoid the batch-to-batch reproducibility problem of polymers[160]. By comparison, small-molecule materials are easy to purify and reproduce with well-defined molecular weights and chemical structures. Before 2017, high PCEs for all-SMOSCs were mainly achieved by using an SMD and a fullerene acceptor, which, owing to the limitations of fullerenes, reached a peak PCE of only 11%[175]. At that time, the development of all-SMOSCs was challenging owing to the limited choice of donor and acceptor materials and the difficulty in controlling the morphology of the photoactive layer, particularly in forming a bicontinuous morphology with two highly crystalline small-molecule materials. The emergence of Y6-type NFAs led to major advances in all-SMOSCs, with the PCE increasing from 9–12% in 2017–2019 (refs. 176–179) to 15–17% after 2020 (refs. 180–182). Popular non-fullerene SMAs used in all-SMOSCs include ITIC and its derivatives, such as IDIC[183] and ITIC-2F[178,179], and the Y6 series of molecules, such as Y6 (ref. 184), N3 (refs. 185,186) and BO-4Cl[187]. As the acceptors have been discussed in a previous section, the following section focuses on the development of SMDs.

Molecular design of small-molecule donors

The molecular design of SMDs, which are typically A–D–A-type or A–π–D–π–A-type polymers, involves consideration of the central core, end groups, π bridge and side chains. The difference between SMDs and SMAs is that the central unit of SMDs cannot be an electron-deficient moiety, because SMDs need to have a HOMO that is much higher in energy than those of SMAs. To date, the benzo-[1,2-*b*:4,5-*b*′]dithiophene (BDT) unit is the most widely used core in SMDs owing to its symmetric planar conjugated structure, which could help improve the molecular packing and charge transport of the SMDs. The use of BDT as an alternative to an oligothiophene SMD core was reported in 2011; the resultant SMD named DCAO3T(BDT)3T (Supplementary Fig. 4) enabled the realization of an all-SMOSC with a PCE of 5.44%[188] (Fig. 2). Following this initial report, other BDT-based SMDs were designed, including DR3TBDT[189] and DR3TSBDT[190] (Supplementary Fig. 4), which were combined with fullerene acceptors, with the resultant devices achieving PCEs of 8–10%. In 2015, a unique SMD named benzo-dithiophene terthiophene rhodanine (BTR) (Figs. 1b and 2) was reported that exhibits nematic liquid crystalline behaviour, which leads to high hole mobilities ($0.1\ cm^2\ V^{-1}\ s^{-1}$ and $1.6 \times 10^{-3}\ cm^2\ V^{-1}\ s^{-1}$ measured using the OFET and space-charge-limited current methods, respectively). Owing to its high

hole mobility, use of BTR in the photoactive layer enabled the fabrication of thick-film OSC devices (with a photoactive layer 300–400-nm thick) with a high fill factor (70%) and a PCE of 8%[191]. The liquid crystalline behaviour of BTR also means that it can be combined with many other acceptor materials and yield good device performance[182,192]. After the emergence of Y6-type SMAs, there was a wave of research on combining reported SMDs with high-performance Y6-SMAs, which quickly increased the PCE of all-SMOSCs to beyond 15%. Representative SMAs used in all-SMOSCs include N3 (refs. 185,186), Y6 (ref. 184), BO-4Cl[193] and BTP-eC9 (ref. 194) (Supplementary Fig. 4). Most recently, the combination of asymmetric SMDs named TB and TB-F (Supplementary Fig. 4) with L8-BO led to a PCE of 17%[195] (Fig. 2 and Table 1).

Other building blocks used to construct SMDs include naphtho[1,2-*b*:5, 6-*b*′]dithiophene[196], porphyrins[197], thieno[2,3-*f*′]benzofuran[198], thienobenzo-dithiophene (TBD)[199] and oligothiophene[200]. One strategy to improve the performance of all-SMOSCs is to use a donor and acceptor with different crystallinities, which can facilitate phase separation. A typical example is the combination of a porphyrin SMD named ZnP-TBO (Supplementary Fig. 4) with red-absorbing SMAs[197]. As morphology control in all-SMOSCs is challenging, device engineering is required to realize the full potential of the materials. For example, the alkylthio-substituted analogue of ZnP-TBO (ZnP-TSEH) (Supplementary Fig. 4) afforded a PCE of 15.88% (15.5% certified) in a ternary device[201], which was further increased to 17.18% through a layer-by-layer (LBL) deposition process with a solid additive to regulate the bulk morphology and vertical phase segregation[202]. Moreover, a volatile-solid-additive strategy has been adopted in Tz6T:eC9-4F binary all-SMOSCs and exhibits advantages over conventional liquid additives[200]. The main problem of commonly used liquid additives (such as 1,8-diiodooctane) is that they have high boiling points (>300 °C) and thus additive residue can remain in the photoactive layer even after completion of device fabrication. By avoiding the liquid additive, the solid-additive approach resulted in improvements in both the PCE and the stability of the device, with >90% of its initial PCE retained after thermal or light soaking for 500 h (ref. 200) (Supplementary Table 1).

Advantages and challenges

Despite the advantages of batch-to-batch reproducibility and molecular-weight control, all-SMOSCs face several challenges (Table 2). First, the morphology of all-small-molecule blends is difficult to control. The two small molecules need to form a bicontinuous network in which the domains are crystalline yet small. Post-treatments such as thermal annealing and solvent vapour annealing are typically needed to achieve a good active-layer morphology and thus efficient all-SMOSCs. However, these treatments, especially solvent vapour annealing, are not suitable for large-scale industrial production. In polymer–fullerene-based or polymer–SMA-based OSCs, the morphology control of the photoactive layer relies on the temperature-dependent aggregation property of the polymer donor, which can form crystalline yet small domains in the BHJ. By contrast, there is no such morphology control mechanism for all-SMOSCs, as there are no examples of SMDs or SMAs that exhibit the same temperature-dependent aggregation property as high-performance polymer donors. The second problem is the low viscosity of the active-layer solution (that is, the solution of the donor and acceptor molecules). For conventional polymer-based OSCs, the polymer component endows the active-layer solution with reasonably high viscosity, which is beneficial for large-area roll-to-roll printing of the photoactive layer. As the photoactive layer of an OSC is quite thin (100–300 nm), it is important to ensure high-quality film formation over a large area, which necessitates high solution viscosity. This problem remains to be solved if all-SMOSCs are to be produced industrially. Finally, the stability of all-SMOSCs has not been widely studied, although there has been a report on device lifetime[200]. The general experience within the OSC research community is that polymer-based materials are more morphologically and thermally stable than are small-molecule materials[146]. By using two small-molecule materials in the photoactive layer, the stability of the photoactive layer, especially the morphological stability, could be questionable. Systematic investigations of the stability of all-SMOSCs are therefore required. However, all-SMOSCs are still at the stage of materials development and efficiency optimization, and answers to these questions might emerge as more material combinations become available.

Multicomponent OSCs

Multicomponent OSCs comprise three or more non-volatile components in one photoactive layer. The initial motivation for multicomponent OSCs was to broaden the absorption of the photoactive layer without using the more complicated tandem OSC structure. Besides broader absorption, researchers also found that multicomponent OSCs could have other attractive features, such as tunable energy levels and V_{OC}, optimized crystallinity and domain size and increased device lifetime. For example, when two fullerene derivatives with different LUMO energy levels are used in a multicomponent OSC, the variation of their ratio can lead to a gradual change of the V_{OC} (refs. 203–205). This result is different from the initial hypothesis that the V_{OC} should be determined by the component with the lowest-energy LUMO, and this phenomenon was later explained by the organic alloy theory (that is, the two acceptor components, if well chosen, could form an organic alloy phase that essentially behaves similar to one component)[206]. Moreover, adding a less-crystalline SMA into binary blends enables the crystallinity and domain size of the blend to be fine-tuned, thus increasing the fill factor[207]. The role of the third component in influencing the morphology has been extensively investigated, as it can not only increase the crystallinity but also reduce it in some cases to balance the electron and hole transport and thus increase the fill factor of the device, as shown in the case of ITIC-4F:ITIC-4Cl[208] (Supplementary Fig. 5). Furthermore, an appropriate SMA third component can increase the overall stability of the device through mechanisms such as morphology lock-in, crystallinity balancing or radical oxidation suppression[209].

Following the emergence of Y6-type SMAs, the development of ternary non-fullerene OSCs greatly accelerated. The most popular type of ternary non-fullerene OSC uses a donor polymer combined with two NFAs, which form organic alloy phases[210,211]. This strategy is particularly effective in fine-tuning the energy levels of the NFAs to form an ideal match with the polymer donor. As there are only limited choices of high-performance polymer donors, represented by PM6 (ref. 75), the energy levels of NFAs need to be tuned to precisely match with those of the high-performance polymer donor in most cases. By using the ternary strategy, researchers could change the ratio of two NFAs to tune the energy levels to form an optimal match with the donor, assuming that the two acceptors form an organic alloy[212].

Another commonly used type of ternary OSC involves a polymer donor, an SMA and a small percentage (typically <3%) of a fullerene acceptor[213]. This type of ternary material can demonstrate the advantages of polymer–SMA-based OSCs, such as small voltage loss, excellent absorption and high efficiency, while also exhibiting the advantages of fullerene acceptors, such as improved charge transport. These properties result in an increase in the V_{OC} and fill factor of the device[214,215].

Table 3 | Single-junction multicomponent organic solar cells with the highest power conversion efficiencies (as of January 2023)

Active-layer configuration	Materials	V_{OC} (V)	J_{SC} (J_{EQE}) (mA cm^{-2})	FF (%)	PCE (%)	Certified PCE (%)	Active area (mm^2)	Masked measurement?	Ref.
Polymer (D)–polymer (A)–polymer (A)	PM6: PY-1S1Se: PY-2Cl	0.914	25.74 (25.15)	77.2	18.2	17.8	10	Yes	238
Polymer (D)–polymer (D)–polymer (A)	PQM-Cl: PTQ10: PY-IT	0.943	24.80 (24.16)	78.9	18.45	NA	4.2	Yes	239
Small molecule (D)–small molecule (A)–small molecule (A)	ZnP-TSEH: 4TIC:6TIC	0.844	26.33 (25.27)	77.31	17.18	17.08	5.142	Yes	202
Small molecule (D)–small molecule (A)–fullerene	BTR-Cl: Y6: $PC_{71}BM$	0.838	23.75 (23.65)	77.11	15.34	14.7	8.636	Yes	240
Small molecule (D)–small molecule (D)–fullerene	DPP-2TTP: DR3TBDTTF: $PC_{71}BM$	0.82	17.78 (17.61)	76.5	11.01	–	NA	Yes	241
Small molecule (D)–small molecule (D)–small molecule (A)	DCAO3TBDTT: DR3TBDTT-S-E: IDIC	0.91	16.37 (15.74)	67.4	10.4	–	4	NA	183
Polymer (D)–small molecule (D)–small molecule (A)	ZR-TT: Y6+3% PJ1	0.811	26.49 (25.20)	72.32	15.54	–	4	NA	242
Polymer (D)–small molecule (A)–small molecule (A)	PM6: L8-BO: BTP-S10	0.898	26.80 (26.19)	80.22	19.26	19.12	6	Yes	77
Polymer (D)–polymer (D)–small molecule (A)	PM6: D18: L8-BO	0.896	26.7 (26.6)	81.9	19.6	19.2	10.4	Yes	81
Polymer (D)–small molecule (A)–fullerene	D18-Cl: N3: $PC_{61}BM$	0.849	28.22 (NA)	78.0	18.69	18.1	4	Yes	243
Polymer (D)–polymer (A)–fullerene	PM6: PY-IT: $PC_{71}BM$	0.942	25.06 (24.69)	69.27	16.36	–	NA	NA	244
Quaternary	PM6: BTP-eC9: BTP-S16: BTP-S17	0.881	27.75 (26.76)	80.83	19.76	19.41	6	Yes	228

The structures of molecules listed in this table are shown in Supplementary Fig. 5. FF, fill factor; J_{EQE}, integrated J_{SC} calculated from external quantum efficiency (EQE) spectra; J_{SC}, short-circuit current density; NA, not available; PCE, power conversion efficiency; V_{OC}, open-circuit voltage.

Moreover, the addition of a small percentage of the fullerene acceptor could even improve the device stability of certain polymer:SMA-based OSCs. For instance, the addition of $PC_{71}BM$ was shown to address the overpurification of the domains and the excessive crystallization tendency of IEICO-4F in the PTB7-Th:IEICO-4F blend[213].

There are, of course, other combinations of the three components. In Table 3, we summarize the device performance of state-of-the-art multicomponent OSCs (in terms of PCE) with different active-layer combinations.

Advantages and challenges

Multicomponent OSCs, including mainly ternary and quaternary devices, offer many attractive features (Table 2). First, they provide more flexibility in the choice and combination of materials and can broaden the absorption of the OSC in a single-junction photoactive layer. Second, using two acceptors that can form an organic alloy phase allows for the energy level and V_{OC} of the device to be linearly tuned with the variation of acceptor ratios; this provides an extremely powerful tool to fine-tune the properties and energy levels of OSCs, which cannot be easily achieved in binary systems. Similarly, multicomponent OSCs provide additional tools to tune the crystallinity, domain size and morphology of BHJ blends, which, if optimized, could lead to a substantial increase in device efficiency and stability.

The main challenge of multicomponent OSCs could be the complicated morphology owing to the involvement of multiple organic material components in one photoactive layer. For some multicomponent OSCs that use multiple polymers, understanding their morphology could be highly challenging, similar to the difficulty in all-polymer blends. However, this challenge can be partially solved by using one polymer donor and two SMAs that can form an organic alloy phase. In this type of ternary OSC, the morphology of the BHJ blends is mostly controlled by the temperature-dependent aggregation property of the polymer donor and the two SMAs essentially behave like one component. The morphological complication of such ternary OSCs is much relieved as their morphology formation is similar to that of conventional binary polymer–small-molecule devices. It is for this reason that such devices are widely used in the OSC research community, which has led to numerous reports of high-performance devices with high efficiency and good device stability.

Other important types of OSCs

One of the weaknesses of BHJ OSCs is that the BHJ morphology could be a kinetically quenched and metastable state, in which the donor and acceptor can undergo demixing and thus morphological change over long-term operation[216]. To overcome the immiscibility problem in BHJ OSCs, researchers have developed single-component OSC (SCOSC) materials that contain both donor and acceptor units covalently linked in one material, reviewed elsewhere[217,218]. One representative example of an SCOSC material is the double-cable polymer named SCP3, which is demonstrated to be highly stable even under rather harsh test conditions[219,220]. For example, SCP3-based SCOSC devices can maintain their performance at the same level for more than 400 h under thermal annealing at 160 °C or continuous light soaking at 90 °C. The development of PSMAs has inspired the development of block copolymers that consist of polymerized donor and acceptor segments; the device based on one of these conjugated block copolymers, PB-b-PY-4, achieved a PCE of up to 13.28%[221] — the highest value reported for SCOSCs so far.

Another technique to fabricate the photoactive layer of OSCs is sequential processing (also known as LBL processing), which could also improve the morphology and large-area processibility of OSCs[222–224].

LBL OSCs are fabricated by processing the donor and then acceptor in two separate layers using orthogonal (or semiorthogonal) solvents[225]. Most importantly, treating the resultant donor–acceptor blend, sometimes a quasi-bilayer structure, by thermal annealing can induce the diffusion of the acceptor into the preformed donor layer, thus forming a pseudo p–i–n structure. LBL OSCs therefore have a different morphology from that of conventional evaporated bilayer OSCs, which is the reason for their much-increased device efficiency[225–227]. The pseudo-bilayer morphology of LBL OSCs leads to many advantages, such as enhanced device stability, thermal stability and mechanical stability for the fabricated devices, and also holds great potential for large-area production.

Outlook

Each type of OSC has its specific advantages, disadvantages and design strategies for future development (Table 2). Comparison of the best performance of the different types of OSCs in terms of efficiency and stability (Table 4) shows that multicomponent OSCs are currently the type with the highest efficiency (with a PCE of 19.7%, or 19.4% certified)[228] and photostability (T_{80} = 20,500 h)[130]. All-PSCs also exhibit relatively good stability (T_{95} = 1,300 h, in which T_{95} is the time for the PCE to decrease by 5%)[166]. The development of polymer–small molecule and multicomponent OSCs (based on SMAs) has been the most rapid, owing to the speed with which ITIC and then Y6-type SMAs have evolved. Thus, although there have been numerous reports of SMA-based OSCs over the past 3–4 years, there have been fewer reports of polymer donors and polymer acceptors, as the synthesis and molecular-weight optimization of polymers is challenging and more time-consuming. This discussion leads to another important topic for OSC commercialization: cost. In general, the cost of OSC materials depends on the number of synthetic steps from readily available raw materials and the overall synthetic yield[229,230]. In addition, polymers (except simple polymers such as P3HT) can have much higher production costs than small molecules, owing to the batch-to-batch variability, which reduces the yield and increases the cost of producing a polymer batch with high performance. For these reasons, the rapid development of SMAs is particularly important, as it generates an enormous pool of material candidates, increasing the probability of finding one that is efficient, stable and low cost.

Regarding progress towards the industrial production of OSCs, polymer–fullerene OSCs are the only ones to have been produced on a large scale by the OSC industry, whereas non-fullerene OSCs are still in the very early stages of industry adoption and face many challenges. Despite the large number of publications on non-fullerene OSCs, there remains a disparity between academic research and the requirements of industry (such as processing conditions and device structure). The academic community and the OSC industry need to collaborate closely to speed up the testing and adoption of newly developed OSC materials by industry. Academic researchers could devote efforts to developing materials that are compatible with industry requirements, whereas industry partners could consider using alternatives to the materials used in conventional fullerene OSCs, such as state-of-the-art non-fullerene materials, in their production lines, which might require adjustment of the production processes. Notable advances towards fulfilling industry requirements include the demonstration of a Y6-based OSC with an inverted structure, enabled by the use of an Ir/IrO_x electron-transporting layer[136] or PEDOT:F hole-transporting layer[139].

An important question to answer is which type of OSC is the most promising direction to pursue for large-scale commercialization of OSC technology. Initially, we believed that all-PSCs were the most promising owing to their superior stability performance compared with other categories. However, the rapid development of multicomponent OSCs has introduced the possibility of developing a hybrid type of OSC that combines the advantageous features of different material types while minimizing their drawbacks. A good example is the popular ternary OSCs based on a polymer–SMA–fullerene material combination. Therefore, rather than restricting research to a single type of material system, researchers should be open to considering a hybrid approach that integrates the strengths of different material types into a single device structure.

With a hybrid approach in mind, we summarize several promising research directions for some types of OSCs discussed herein. First, all-PSCs have already demonstrated good stability, which is probably sufficient for indoor applications. However, the absorption of window of most all-PSC material blends is mainly designed for outdoor application. Therefore, an important research direction is to design polymer acceptors that absorb light with wavelengths in the range 400–700 nm

Table 4 | Comparison of the best performance of different types of organic solar cells

Category	PCE (%)[a]	Photostability[b]	Relative development pace in terms of efficiency	Progress towards industrial production
Polymer–fullerene	11–12 (ref. 42)	T_{80}=14,250 h (ref. 38)	Very slow; no progress in efficiency after 2016	Mature stage
Polymer–small molecule	18.9–19.0 (ref. 97)	Extrapolated T_{80}=11,000 h (ref. 134)	Very fast; PCE increased from 7% in 2015 (ref. 64) to 15% in 2019 (ref. 76) and 19% in 2022 (ref. 97)	Early stage
All-polymer	17.6–18.1 (ref. 164)	T_{95}=1,300 h (ref. 166)	Moderate, owing to adoption of SMA units into polymers; moderate increase in PCE before 2020 (11.7% in 2019)[153] and rapid after 2020 (18% in 2022)[164]	Early stage
All-small molecule	17 (ref. 195)	T_{92}=500 h (ref. 200)	Slow, owing to the challenge of morphology control; PCE increased from 8% in 2015 to 15% in 2021 and 17% in 2022	Early stage
Multicomponent	19.4 (ref. 228)	T_{90}=2,000 h, extrapolated T_{80}=20,500 h (ref. 130)	Fast, owing to rapid development of SMAs	Early stage

SMA, small-molecule acceptor; PCE, power conversion efficiency; T_{80}, the time for the PCE to decrease by 20%; T_{90}, the time for the PCE to decrease by 10%; T_{92}, the time for the PCE to decrease by 8%; T_{95}, the time for the PCE to decrease by 5%. [a]Certified PCE except for all-small-molecule organic solar cells. [b]Photostability under simulated AM1.5G (a global horizontal irradiance spectrum generally used in terrestrial solar cell research).

to achieve all-PSCs with high indoor efficiencies. One possibility is to borrow molecular design concepts from SMAs designed for indoor applications and use those structural units as monomers for polymer acceptors. Another possibility is to design a hybrid material blend that includes a polymer donor, polymer acceptor and SMA. The goal is to maintain the excellent morphological stability of all-PSC systems while incorporating an SMA that can enhance absorption in the indoor lighting spectral range.

The priority in polymer–SMA OSC research should be improving the stability. The acidic hydrogen on the linking ethylene group of typical SMAs has already been identified as the probable cause of the stability issue, and extensive research efforts have been spent on modifying the linking group and should be further pursued. Given the rapid pace of the development of SMA materials, we would not be surprised to see SMA material innovations that solve the stability issue. Progress in the molecular design of SMAs to increase the stability can also immediately benefit all-PSCs, as polymer acceptors are usually based on monomers with similar structures to those of the latest SMA materials. Conversely, polymer–SMA OSCs can benefit from progress in all-PSCs by linking SMA materials into dimers[231,232] or oligomers[233,234] to improve the stability. In some areas, research on all-PSCs and polymer–SMA OSCs is mutually beneficial, and these two types of OSCs will probably progress in a balanced manner.

Currently, polymer–small molecule OSCs achieve high efficiency at the expense of stability. Owing to the lack of understanding of the molecular assembly in blends, controlling the morphology of OSCs remains challenging and relies largely on trial-and-error-based approaches for molecular design and device engineering. Understanding the molecular assembly pathways might provide insights to help balance the stability and device performance. At present, high-throughput screening technology has been widely used in organic synthesis and drug discovery to minimize human resources and expand the chemical space of exploration, whereas there are only a few examples of applications in OSC research. For example, self-driving laboratories based on an autonomous robotic experimental platform were combined with machine-learning or artificial intelligence models to automate OSC fabrication and characterization to optimize the PCE and stability[235–237]. Further integration of high-throughput screening with artificial intelligence and/or machine-learning methods could enable mutual feedback between molecular design, fabrication processes and device performance. Such developments could help to realize the industrial production and commercialization of OSC technology.

Published online: 15 December 2023

References

1. Yuen, S. Global Installed PV Capacity Passes 1.18TW — IEA. *PV-Tech* https://www.pv-tech.org/global-installed-pv-capacity-passes-1-18tw-iea/#:~:Text=It%20reached%20about%201.2TW,International%20Energy%20Agency%20(IEA) (2023).
2. The Brainy Insights. Solar Cell Market Size by Material (Crystalline [N Material and P Material] and Thin Film), Product (BSF, PERC/PERL/PERT/TOPCON, HJT, IBC & MWT and Others), Technology (Monocrystalline, Polycrystalline, Cadmium Telluride (CDTE), Amorphous Silicon (A-Si) and Copper Indium Gallium Diselenide), End User (Residential, Commercial and Utility), Regions, Global Industry Analysis, Share, Growth, Trends, and Forecast 2023 to 2032. *The Brainy Insights* http:\\www.thebrainyinsights.com/report/solar-cell-market-13707#summary (2023).
3. Anctil, A. et al. Cumulative energy demand for small molecule and polymer photovoltaics. *Prog. Photovolt. Res. Appl.* **21**, 1541–1554 (2013).
4. Anctil, A. et al. Net energy and cost benefit of transparent organic solar cells in building-integrated applications. *Appl. Energy* **261**, 114429 (2020).
5. Zhou, Z. & Carbajales-Dale, M. Assessing the photovoltaic technology landscape: efficiency and energy return on investment (EROI). *Energy Environ. Sci.* **11**, 603–608 (2018).
6. García-Valverde, R. et al. Life cycle analysis of organic photovoltaic technologies. *Prog. Photovolt. Res. Appl.* **18**, 535–558 (2010).
7. Roes, A. L. et al. Ex-ante environmental and economic evaluation of polymer photovoltaics. *Prog. Photovolt. Res. Appl.* **17**, 372–393 (2009).
8. Heeger, A. J. 25th anniversary article: bulk heterojunction solar cells: understanding the mechanism of operation. *Adv. Mater.* **26**, 10–28 (2014).
9. Lewis, N. S. Toward cost-effective solar energy use. *Science* **315**, 798–801 (2007).
10. Jean, J. et al. Pathways for solar photovoltaics. *Energy Environ. Sci.* **8**, 1200–1219 (2015).
11. Martin, B. et al. Techno-economic analysis of roll-to-roll production of perovskite modules using radiation thermal processes. *Appl. Energy* **307**, 118200 (2022).
12. Osedach, T. P. et al. Effect of synthetic accessibility on the commercial viability of organic photovoltaics. *Energy Environ. Sci.* **6**, 711–718, (2013).
13. Carlson, D. E. & Wronski, C. R. Amorphous silicon solar cell. *Appl. Phys. Lett.* **28**, 671–673 (1976).
14. Lungenschmied, C. et al. Flexible, long-lived, large-area, organic solar cells. *Sol. Energy Mater. Sol. Cell* **91**, 379–384 (2007).
15. Brus, V. V. et al. Solution-processed semitransparent organic photovoltaics: from molecular design to device performance. *Adv. Mater.* **31**, 1900904 (2019).
16. Forberich, K. et al. Efficiency limits and color of semitransparent organic solar cells for application in building-integrated photovoltaics. *Energy Technol.* **3**, 1051–1058 (2015).
17. Park, S. et al. Self-powered ultra-flexible electronics via nano-grating-patterned organic photovoltaics. *Nature* **561**, 516–521 (2018).
18. Jeon, K. E. et al. BLE beacons for internet of things applications: survey, challenges, and opportunities. *IEEE Internet Things J.* **5**, 811–828 (2018).
19. Gubbi, J. et al. Internet of Things (IoT): a vision, architectural elements, and future directions. *Future Gener. Comput. Syst.* **29**, 1645–1660 (2013).
20. Freitag, M. et al. Dye-sensitized solar cells for efficient power generation under ambient lighting. *Nat. Photon.* **11**, 372–378 (2017).
21. Mathews, I. et al. Technology and market perspective for indoor photovoltaic cells. *Joule* **3**, 1415–1426 (2019).
22. Foti, M. et al. Efficient flexible thin film silicon module on plastics for indoor energy harvesting. *Sol. Energy Mater. Sol. Cell* **130**, 490–494 (2014).
23. Yue, X. et al. Development of an indoor photovoltaic energy harvesting module for autonomous sensors in building air quality applications. *IEEE Internet Things J.* **4**, 2092–2103 (2017).
24. Lee, C. et al. Over 30% efficient indoor organic photovoltaics enabled by morphological modification using two compatible non-fullerene acceptors. *Adv. Energy Mater.* **12**, 2200275 (2022).
25. Ma, L.-K. et al. High-efficiency indoor organic photovoltaics with a band-aligned interlayer. *Joule* **4**, 1486–1500 (2020).
26. Zhang, T. et al. A medium-bandgap nonfullerene acceptor enabling organic photovoltaic cells with 30% efficiency under indoor artificial light. *Adv. Mater.* **34**, e2207009 (2022).
27. Bai, F. et al. A highly crystalline non-fullerene acceptor enabling efficient indoor organic photovoltaics with high EQE and fill factor. *Joule* **5**, 1231–1245 (2021).
28. Saeed, M. A. et al. 2D MXene additive-induced treatment enabling high-efficiency indoor organic photovoltaics. *Adv. Opt. Mater.* **11**, 2202135 (2022).
29. Mori, S. et al. Investigation of the organic solar cell characteristics for indoor LED light applications. *Jpn. J. Appl. Phys.* **54**, 071602 (2015).
30. Yu, G. et al. Polymer photovoltaic cells: enhanced efficiencies via a network of internal donor–acceptor heterojunctions. *Science* **270**, 1789–1791 (1995).
31. Halls, J. J. M. et al. Efficient photodiodes from interpenetrating polymer networks. *Nature* **376**, 498–500 (1995).
32. Gaspar, H. et al. Recent developments in the optimization of the bulk heterojunction morphology of polymer: fullerene solar cells. *Materials* **11**, 2560 (2018).
33. Liu, Y. et al. Recent progress in organic solar cells (part I: material science). *Sci. China Chem.* **65**, 224–268 (2022).
34. Fu, H. et al. Polymer donors for high-performance non-fullerene organic solar cells. *Angew. Chem. Int. Ed.* **58**, 4442–4453 (2019).
35. Schilinsky, P. et al. Recombination and loss analysis in polythiophene based bulk heterojunction photodetectors. *Appl. Phys. Lett.* **81**, 3885–3887 (2002).
36. Mühlbacher, D. et al. High photovoltaic performance of a low-bandgap polymer. *Adv. Mater.* **18**, 2884–2889 (2006).
37. Liang, Y. et al. For the bright future — bulk heterojunction polymer solar cells with power conversion efficiency of 7.4%. *Adv. Mater.* **22**, E135–E138 (2010).
38. Liu, Q. et al. Circumventing UV light induced nanomorphology disorder to achieve long lifetime PTB7-Th:PCBM based solar cells. *Adv. Energy Mater.* **7**, 1701201 (2017).
39. Liu, Y. et al. Aggregation and morphology control enables multiple cases of high-efficiency polymer solar cells. *Nat. Commun.* **5**, 5293 (2014).
40. Zhou, P. et al. Thiophene-fused benzothiadiazole: a strong electron–acceptor unit to build D–A copolymer for highly efficient polymer solar cells. *Chem. Mater.* **26**, 3495–3501 (2014).
41. Chen, Z. et al. Low band-gap conjugated polymers with strong interchain aggregation and very high hole mobility towards highly efficient thick-film polymer solar cells. *Adv. Mater.* **26**, 2586–2591 (2014).
42. Zhao, J. et al. Efficient organic solar cells processed from hydrocarbon solvents. *Nat. Energy* **1**, 15027 (2016).
43. Lu, L. et al. Recent advances in bulk heterojunction polymer solar cells. *Chem. Rev.* **115**, 12666–12731 (2015).

44. Nian, L. et al. Photoconductive cathode interlayer for highly efficient inverted polymer solar cells. *J. Am. Chem. Soc.* **137**, 6995–6998 (2015).
45. He, Z. et al. Single-junction polymer solar cells with high efficiency and photovoltage. *Nat. Photon.* **9**, 174–179 (2015).
46. Wan, Q. et al. 10.8% Efficiency polymer solar cells based on PTB7-Th and PC71BM via binary solvent additives treatment. *Adv. Funct. Mater.* **26**, 6635–6640 (2016).
47. von Hauff, E. et al. Study of field effect mobility in PCBM films and P3HT:PCBM blends. *Sol. Energy Mater. Sol. Cell* **87**, 149–156 (2005).
48. Gao, D. et al. Evolution of the electron mobility in polymer solar cells with different fullerene acceptors. *ACS Appl. Mater. Interfaces* **5**, 8038–8043 (2013).
49. Fenta, A. D. et al. High efficiency organic photovoltaics with a thick (300 nm) bulk heterojunction comprising a ternary composition of a PFT polymer–PC71BM fullerene–IT4F nonfullerene acceptor. *ACS Appl. Energy Mater.* **4**, 5274–5285 (2021).
50. Zhang, D. et al. Recent progress in thick-film organic photovoltaic devices: materials, devices, and processing. *SusMat* **1**, 4–23 (2021).
51. Amb, C. M. et al. Aesthetically pleasing conjugated polymer:fullerene blends for blue-green solar cells via roll-to-roll processing. *ACS Appl. Mater. Interfaces* **4**, 1847–1853 (2012).
52. Azzopardi, B. et al. Economic assessment of solar electricity production from organic-based photovoltaic modules in a domestic environment. *Energy Environ. Sci.* **4**, 3741–3753, (2011).
53. Liu, J. et al. Emerging electronic applications of fullerene derivatives: an era beyond OPV. *J. Mater. Chem. C* **9**, 16143–16163 (2021).
54. Dey, S. Recent progress in molecular design of fused ring electron acceptors for organic solar cells. *Small* **15**, 1900134 (2019).
55. Jones, B. A. et al. High-mobility air-stable n-type semiconductors with processing versatility: dicyanoperylene-3,4:9,10-bis(dicarboximides). *Angew. Chem. Int. Ed.* **43**, 6363–6366 (2004).
56. Yan, Q. et al. Towards rational design of organic electron acceptors for photovoltaics: a study based on perylenediimide derivatives. *Chem. Sci.* **4**, 4389–4394 (2013).
57. Weitz, R. T. et al. Organic n-channel transistors based on core-cyanated perylene carboxylic diimide derivatives. *J. Am. Chem. Soc.* **130**, 4637–4645 (2008).
58. Kim, S. H. et al. Organic field-effect transistors using perylene. *Opt. Mater.* **21**, 439–443 (2003).
59. Li, C. et al. Polyphenylene-based materials for organic photovoltaics. *Chem. Rev.* **110**, 6817–6855 (2010).
60. Zhan, X. et al. Rylene and related diimides for organic electronics. *Adv. Mater.* **23**, 268–284 (2011).
61. Schmidt-Mende, L. et al. Self-organized discotic liquid crystals for high-efficiency organic photovoltaics. *Science* **293**, 1119–1122 (2001).
62. Zhang, M. et al. Perylene-diimide derived organic photovoltaic materials. *Sci. China Chem.* **65**, 462–485 (2022).
63. Cao, J. & Yang, S. Progress in perylene diimides for organic solar cell applications. *RSC Adv.* **12**, 6966–6973 (2022).
64. Lin, Y. et al. An electron acceptor challenging fullerenes for efficient polymer solar cells. *Adv. Mater.* **27**, 1170–1174 (2015).
65. Jia, B. et al. Enhancing the performance of a fused-ring electron acceptor by unidirectional extension. *J. Am. Chem. Soc.* **141**, 19023–19031 (2019).
66. Wang, J. et al. Effect of isomerization on high-performance nonfullerene electron acceptors. *J. Am. Chem. Soc.* **140**, 9140–9147 (2018).
67. Cui, Y. et al. Achieving over 15% efficiency in organic photovoltaic cells via copolymer design. *Adv. Mater.* **31**, 1808356 (2019).
68. Li, S. et al. A wide band gap polymer with a deep highest occupied molecular orbital level enables 14.2% efficiency in polymer solar cells. *J. Am. Chem. Soc.* **140**, 7159–7167 (2018).
69. Chang, Y. et al. Progress and prospects of thick-film organic solar cells. *J. Mater. Chem. A* **9**, 3125–3150 (2021).
70. Wang, J. & Zhan, X. Fused-ring electron acceptors for photovoltaics and beyond. *Acc. Chem. Res.* **54**, 132–143 (2021).
71. Liu, J. et al. Fast charge separation in a non-fullerene organic solar cell with a small driving force. *Nat. Energy* **1**, 16089 (2016).
72. Zhao, J. et al. High-efficiency non-fullerene organic solar cells enabled by a difluorobenzothiadiazole-based donor polymer combined with a properly matched small molecule acceptor. *Energy Environ. Sci.* **8**, 520–525 (2015).
73. Hu, H. et al. Design of donor polymers with strong temperature-dependent aggregation property for efficient organic photovoltaics. *Acc. Chem. Res.* **50**, 2519–2528 (2017).
74. Qian, D. et al. Design, application, and morphology study of a new photovoltaic polymer with strong aggregation in solution state. *Macromolecules* **45**, 9611–9617 (2012).
75. Zhang, M. et al. A large-bandgap conjugated polymer for versatile photovoltaic applications with high performance. *Adv. Mater.* **27**, 4655–4660 (2015).
76. Yuan, J. et al. Single-junction organic solar cell with over 15% efficiency using fused-ring acceptor with electron-deficient core. *Joule* **3**, 1140–1151 (2019).
77. Zhan, L. et al. Manipulating charge transfer and transport via intermediary electron acceptor channels enables 19.3% efficiency organic photovoltaics. *Adv. Energy Mater.* **12**, 2201076 (2022).
78. Jiang, K. et al. Suppressed recombination loss in organic photovoltaics adopting a planar-mixed heterojunction architecture. *Nat. Energy* **7**, 1076–1086 (2022).
79. He, C. et al. Manipulating the D:A interfacial energetics and intermolecular packing for 19.2% efficiency organic photovoltaics. *Energy Environ. Sci.* **15**, 2537–2544 (2022).
80. Sun, R. et al. Single-junction organic solar cells with 19.17% efficiency enabled by introducing one asymmetric guest acceptor. *Adv. Mater.* **34**, 2110147 (2022).
81. Zhu, L. et al. Single-junction organic solar cells with over 19% efficiency enabled by a refined double-fibril network morphology. *Nat. Mater.* **21**, 656–663 (2022).
82. Li, P. et al. Banana-shaped electron acceptors with an electron-rich core fragment and 3D packing capability. *Carbon Energy* **5**, e250 (2023).
83. Abbas, Z. et al. Optimized vertical phase separation via systematic Y6 inner side-chain modulation for non-halogen solvent processed inverted organic solar cells. *Nano Energy* **101**, 107574 (2022).
84. Li, D. et al. Asymmetric non-fullerene small-molecule acceptors toward high-performance organic solar cells. *ACS Cent. Sci.* **7**, 1787–1797 (2021).
85. Li, C. et al. Non-fullerene acceptors with branched side chains and improved molecular packing to exceed 18% efficiency in organic solar cells. *Nat. Energy* **6**, 605–613 (2021).
86. Hofinger, J. et al. Understanding the low voltage losses in high-performance non-fullerene acceptor-based organic solar cells. *Mater. Adv.* **2**, 4291–4302 (2021).
87. Zheng, Z. et al. Efficient charge transfer and fine-tuned energy level alignment in a THF-processed fullerene-free organic solar cell with 11.3% efficiency. *Adv. Mater.* **29**, 1604241 (2017).
88. Zhu, L. et al. Small exciton binding energies enabling direct charge photogeneration towards low-driving-force organic solar cells. *Angew. Chem. Int. Ed.* **60**, 15348–15353 (2021).
89. Han, G. & Yi, Y. Molecular insight into efficient charge generation in low-driving-force nonfullerene organic solar cells. *Acc. Chem. Res.* **55**, 869–877 (2022).
90. Li, X. et al. Recent advances in Y6-based semiconductors: performance in solar cells, crystallography, and electronic structure. *ChemPlusChem* **86**, 700–708 (2021).
91. Gao, W. et al. Achieving 19% power conversion efficiency in planar-mixed heterojunction organic solar cells using a pseudosymmetric electron acceptor. *Adv. Mater.* **34**, 2202089 (2022).
92. Liu, S. et al. High-efficiency organic solar cells with low non-radiative recombination loss and low energetic disorder. *Nat. Photon.* **14**, 300–305 (2020).
93. Zhou, Z. et al. Subtle molecular tailoring induces significant morphology optimization enabling over 16% efficiency organic solar cells with efficient charge generation. *Adv. Mater.* **32**, 1906324 (2020).
94. Song, Y. et al. Fused-heterocycle engineering on asymmetric non-fullerene acceptors enables organic solar cells approaching 29 mA/cm^2 short-circuit current density. *Chem. Eng. J.* **430**, 132830 (2022).
95. Jiang, K. et al. Alkyl chain tuning of small molecule acceptors for efficient organic solar cells. *Joule* **3**, 3020–3033 (2019).
96. Hong, L. et al. Eco-compatible solvent-processed organic photovoltaic cells with over 16% efficiency. *Adv. Mater.* **31**, 1903441 (2019).
97. Wei, Y. et al. Binary organic solar cells breaking 19% via manipulating the vertical component distribution. *Adv. Mater.* **34**, 2204718 (2022).
98. Chai, G. et al. Fine-tuning of side-chain orientations on nonfullerene acceptors enables organic solar cells with 17.7% efficiency. *Energy Environ. Sci.* **14**, 3469–3479 (2021).
99. Zhang, J. et al. Alkyl-chain branching of non-fullerene acceptors flanking conjugated side groups toward highly efficient organic solar cells. *Adv. Energy Mater.* **11**, 2102596 (2021).
100. Kong, X. et al. The effect of alkyl substitution position of thienyl outer side chains on photovoltaic performance of A–DA′D–A type acceptors. *Energy Environ. Sci.* **15**, 2011–2020 (2022).
101. Shang, A. et al. Over 18% binary organic solar cells enabled by isomerization of non-fullerene acceptors with alkylthiophene side chains. *Sci. China Chem.* **65**, 1758–1766 (2022).
102. Chen, Y. et al. Asymmetric alkoxy and alkyl substitution on nonfullerene acceptors enabling high-performance organic solar cells. *Adv. Energy Mater.* **11**, 2003141 (2021).
103. Murugan, P. et al. Fused ring A–DA′D–A (Y-series) non-fullerene acceptors: recent developments and design strategies for organic photovoltaics. *J. Mater. Chem. A* **10**, 17968–17987 (2022).
104. Zhao, J. et al. Recent advances in high-performance organic solar cells enabled by acceptor–donor–acceptor–donor–acceptor (A–DA′D–A) type acceptors. *Mater. Chem. Front.* **4**, 3487–3504 (2020).
105. Zhang, Y. et al. Recent progress of Y6-derived asymmetric fused ring electron acceptors. *Adv. Funct. Mater.* **32**, 2205115 (2022).
106. Li, X. et al. Benzo[1,2-b:4,5-b′]difuran based polymer donor for high-efficiency (>16%) and stable organic solar cells. *Adv. Energy Mater.* **12**, 2103684 (2022).
107. Chen, H. et al. 17.1%-efficient eco-compatible organic solar cells from a dissymmetric 3D network acceptor. *Angew. Chem. Int. Ed.* **60**, 3238–3246 (2021).
108. Li, S. et al. Asymmetric electron acceptors for high-efficiency and low-energy-loss organic photovoltaics. *Adv. Mater.* **32**, 2001160 (2020).
109. Luo, Z. et al. Fine-tuning energy levels via asymmetric end groups enables polymer solar cells with efficiencies over 17%. *Joule* **4**, 1236–1247 (2020).
110. Mishra, A. & Sharma, G. D. Harnessing the structure–performance relationships in designing non-fused ring acceptors for organic solar cells. *Angew. Chem. Int. Ed.* **62**, e202219245 (2023).
111. Gao, H. et al. Recent progress in non-fused ring electron acceptors for high performance organic solar cells. *Ind. Chem. Mater.* **1**, 60–78 (2023).
112. Peng, W. et al. Simple-structured NIR-absorbing small-molecule acceptors with a thiazolothiazole core: multiple noncovalent conformational locks and D–A effect for efficient OSCs. *ACS Appl. Mater. Interfaces* **11**, 48128–48133 (2019).
113. Peng, W. et al. Simple-structured small molecule acceptors constructed by a weakly electron-deficient thiazolothiazole core for high-efficiency non-fullerene organic solar cells. *J. Mater. Chem. A* **6**, 24267–24276 (2018).

114. Yan, C. et al. Non-fullerene acceptors for organic solar cells. *Nat. Rev. Mater.* **3**, 18003 (2018).
115. Fei, Z. et al. An alkylated indacenodithieno[3,2-b]thiophene-based nonfullerene acceptor with high crystallinity exhibiting single junction solar cell efficiencies greater than 13% with low voltage losses. *Adv. Mater.* **30**, 1705209 (2018).
116. Huang, C. et al. Highly efficient organic solar cells based on S,N-heteroacene non-fullerene acceptors. *Chem. Mater.* **30**, 5429–5434 (2018).
117. Liu, Y. et al. Exploiting noncovalently conformational locking as a design strategy for high performance fused-ring electron acceptor used in polymer solar cells. *J. Am. Chem. Soc.* **139**, 3356–3359 (2017).
118. Yao, H. et al. Design and synthesis of a low bandgap small molecule acceptor for efficient polymer solar cells. *Adv. Mater.* **28**, 8283–8287 (2016).
119. Huang, H. et al. Noncovalently fused-ring electron acceptors with near-infrared absorption for high-performance organic solar cells. *Nat. Commun.* **10**, 3038 (2019).
120. Pang, S. et al. Nonfused nonfullerene acceptors with an A–D–A′–D–A framework and a benzothiadiazole core for high-performance organic solar cells. *ACS Appl. Mater. Interfaces* **12**, 16531–16540 (2020).
121. Ma, D.-L. et al. Unsymmetrically chlorinated non-fused electron acceptor leads to high-efficiency and stable organic solar cells. *Angew. Chem. Int. Ed.* **62**, e202214931 (2023).
122. Kaiser, C. et al. A universal Urbach rule for disordered organic semiconductors. *Nat. Commun.* **12**, 3988 (2021).
123. Chen, X.-K. et al. A unified description of non-radiative voltage losses in organic solar cells. *Nat. Energy* **6**, 799–806 (2021).
124. Liu, Q. & Vandewal, K. Understanding and suppressing non-radiative recombination losses in non-fullerene organic solar cells. *Adv. Mater.* **35**, 2302452 (2023).
125. Badgujar, S. et al. Highly efficient and thermally stable fullerene-free organic solar cells based on a small molecule donor and acceptor. *J. Mater. Chem. A* **4**, 16335–16340 (2016).
126. Holliday, S. et al. High-efficiency and air-stable P3HT-based polymer solar cells with a new non-fullerene acceptor. *Nat. Commun.* **7**, 11585 (2016).
127. Gasparini, N. et al. Exploiting ternary blends for improved photostability in high-efficiency organic solar cells. *ACS Energy Lett.* **5**, 1371–1379 (2020).
128. Gasparini, N. et al. Burn-in free nonfullerene-based organic solar cells. *Adv. Energy Mater.* **7**, 1700770 (2017).
129. Wang, W. et al. Exploring the chemical interaction between diiodooctane and PEDOT-PSS electrode for metal electrode-free nonfullerene organic solar cells. *ACS Appl. Mater. Interfaces* **12**, 3800–3805 (2020).
130. Wang, Y. et al. Stability of nonfullerene organic solar cells: from built-in potential and interfacial passivation perspectives. *Adv. Energy Mater.* **9**, 1900157 (2019).
131. Guo, J. et al. Suppressing photo-oxidation of non-fullerene acceptors and their blends in organic solar cells by exploring material design and employing friendly stabilizers. *J. Mater. Chem. A* **7**, 25088–25101 (2019).
132. Liu, H. et al. A ring-locking strategy to enhance the chemical and photochemical stability of A–D–A-type non-fullerene acceptors. *J. Mater. Chem. A* **9**, 1080–1088 (2021).
133. Bertrandie, J. et al. Air-processable and thermally stable hole transport layer for non-fullerene organic solar cells. *ACS Appl. Energy Mater.* **5**, 1023–1030 (2022).
134. Du, X. et al. Efficient polymer solar cells based on non-fullerene acceptors with potential device lifetime approaching 10 years. *Joule* **3**, 215–226 (2019).
135. Du, X. et al. Unraveling the microstructure-related device stability for polymer solar cells based on nonfullerene small-molecular acceptors. *Adv. Mater.* **32**, 1908305 (2020).
136. Li, Y. et al. Lifetime over 10,000 hours for organic solar cells with Ir/IrO_x electron-transporting layer. *Nat. Commun.* **14**, 1241 (2023).
137. Cameron, J. & Skabara, P. J. The damaging effects of the acidity in PEDOT:PSS on semiconductor device performance and solutions based on non-acidic alternatives. *Mater. Horiz.* **7**, 1759–1772 (2020).
138. Dong, X. et al. Two-in-one alcohol-processed PEDOT electrodes produced by solvent exchange for organic solar cells. *Energy Environ. Sci.* **16**, 1511–1519 (2023).
139. Jiang, Y. et al. An alcohol-dispersed conducting polymer complex for fully printable organic solar cells with improved stability. *Nat. Energy* **7**, 352–359 (2022).
140. Yu, G. & Heeger, A. J. Charge separation and photovoltaic conversion in polymer composites with internal donor/acceptor heterojunctions. *J. Appl. Phys.* **78**, 4510–4515 (1995).
141. Fan, Q. et al. Mechanically robust all-polymer solar cells from narrow band gap acceptors with hetero-bridging atoms. *Joule* **4**, 658–672 (2020).
142. Sun, H. et al. High-performance n-type polymer semiconductors: applications, recent development, and challenges. *Chem* **6**, 1310–1326 (2020).
143. Yan, H. et al. A high-mobility electron-transporting polymer for printed transistors. *Nature* **457**, 679–686 (2009).
144. Zhan, X. et al. A high-mobility electron-transport polymer with broad absorption and its use in field-effect transistors and all-polymer solar cells. *J. Am. Chem. Soc.* **129**, 7246–7247 (2007).
145. Lee, C. et al. Recent advances, design guidelines, and prospects of all-polymer solar cells. *Chem. Rev.* **119**, 8028–8086 (2019).
146. Wang, G. et al. All-polymer solar cells: recent progress, challenges, and prospects. *Angew. Chem. Int. Ed.* **58**, 4129–4142 (2019).
147. Yang, J. et al. Aromatic-diimide-based n-type conjugated polymers for all-polymer solar cell applications. *Adv. Mater.* **31**, 1804699 (2019).
148. Hwang, Y.-J. et al. 7.7% Efficient all-polymer solar cells. *Adv. Mater.* **27**, 4578–4584 (2015).
149. Guo, Y. et al. A vinylene-bridged perylenediimide-based polymeric acceptor enabling efficient all-polymer solar cells processed under ambient conditions. *Adv. Mater.* **28**, 8483–8489 (2016).
150. Guo, Y. et al. Improved performance of all-polymer solar cells enabled by naphthodiperylenetetraimide-based polymer acceptor. *Adv. Mater.* **29**, 1700309 (2017).
151. Guo, X. & Watson, M. D. Conjugated polymers from naphthalene bisimide. *Org. Lett.* **10**, 5333–5336 (2008).
152. Zhou, K. et al. Morphology control in high-efficiency all-polymer solar cells. *InfoMat* **4**, e12270 (2022).
153. Zhu, L. et al. Aggregation-induced multilength scaled morphology enabling 11.76% efficiency in all-polymer solar cells using printing fabrication. *Adv. Mater.* **31**, 1902899 (2019).
154. Gao, L. et al. All-polymer solar cells based on absorption-complementary polymer donor and acceptor with high power conversion efficiency of 8.27%. *Adv. Mater.* **28**, 1884–1890 (2016).
155. Zhang, Z.-G. & Li, Y. Polymerized small-molecule acceptors for high-performance all-polymer solar cells. *Angew. Chem. Int. Ed.* **60**, 4422–4433 (2021).
156. Zhao, R. et al. Organoboron polymer for 10% efficiency all-polymer solar cells. *Chem. Mater.* **32**, 1308–1314 (2020).
157. Xu, X. et al. Highly efficient all-polymer solar cells enabled by p-doping of the polymer donor. *ACS Energy Lett.* **5**, 2434–2443 (2020).
158. Feng, K. et al. High-performance all-polymer solar cells enabled by n-type polymers with an ultranarrow bandgap down to 1.28 eV. *Adv. Mater.* **32**, 2001476 (2020).
159. Zhang, Z.-G. et al. Constructing a strongly absorbing low-bandgap polymer acceptor for high-performance all-polymer solar cells. *Angew. Chem. Int. Ed.* **56**, 13503–13507 (2017).
160. Wang, W. et al. Controlling molecular mass of low-band-gap polymer acceptors for high-performance all-polymer solar cells. *Joule* **4**, 1070–1086 (2020).
161. Jia, T. et al. 14.4% efficiency all-polymer solar cell with broad absorption and low energy loss enabled by a novel polymer acceptor. *Nano Energy* **72**, 104718 (2020).
162. Luo, Z. et al. Precisely controlling the position of bromine on the end group enables well-regular polymer acceptors for all-polymer solar cells with efficiencies over 15%. *Adv. Mater.* **32**, 2005942 (2020).
163. Wang, J. et al. A new polymer donor enables binary all-polymer organic photovoltaic cells with 18% efficiency and excellent mechanical robustness. *Adv. Mater.* **34**, 2205009 (2022).
164. Zhang, T. et al. Suppressing the energetic disorder of all-polymer solar cells enables over 18% efficiency. *Energy Environ. Sci.* **16**, 1581–1589 (2023).
165. Yang, X. et al. Ternary all-polymer solar cells with efficiency up to 18.14% employing a two-step sequential deposition. *Adv. Mater.* **35**, e2209350 (2022).
166. Zhang, J. et al. π-Extended conjugated polymer acceptor containing thienylene–vinylene–thienylene unit for high-performance thick-film all-polymer solar cells with superior long-term stability. *Adv. Energy Mater.* **11**, 2102559 (2021).
167. Li, Z. et al. A universal strategy via polymerizing non-fullerene small molecule acceptors enables efficient all-polymer solar cells with > 1 year excellent thermal stability. *Chem. Eng. J.* **430**, 132711 (2022).
168. Sun, R. et al. Achieving over 17% efficiency of ternary all-polymer solar cells with two well-compatible polymer acceptors. *Joule* **5**, 1548–1565 (2021).
169. Kim, T. et al. Flexible, highly efficient all-polymer solar cells. *Nat. Commun.* **6**, 8547 (2015).
170. Lee, J.-W. et al. Sequentially regular polymer acceptors featuring flexible spacers for high-performance and mechanically robust all-polymer solar cells. *Energy Environ. Sci.* **15**, 4672–4685 (2022).
171. Zeng, A. et al. A chlorinated donor polymer achieving high-performance organic solar cells with a wide range of polymer molecular weight. *Adv. Funct. Mater.* **31**, 2102413 (2021).
172. Liang, Y. et al. Organic solar cells using oligomer acceptors for improved stability and efficiency. *Nat. Energy* **7**, 1180–1190 (2022).
173. Zhao, C. et al. 18.1% Ternary all-polymer solar cells sequentially processed from hydrocarbon solvent with enhanced stability. *Adv. Energy Mater.* **13**, 2300904 (2023).
174. Zhao, C. et al. An improved performance of all polymer solar cells enabled by sequential processing via non-halogenated solvents. *Nano Energy* **104**, 107872 (2022).
175. Deng, D. et al. Fluorination-enabled optimal morphology leads to over 11% efficiency for inverted small-molecule organic solar cells. *Nat. Commun.* **7**, 13740 (2016).
176. Zhang, S. et al. Influence of the replacement of alkoxyl with alkylthienyl on photovoltaic properties of two small molecule donors for organic solar cells. *Sci. China Chem.* **60**, 1340–1348 (2017).
177. Yang, L. et al. New wide band gap donor for efficient fullerene-free all-small-molecule organic solar cells. *J. Am. Chem. Soc.* **139**, 1958–1966 (2017).
178. Li, X. et al. A small molecule donor containing a non-fused ring core for all-small-molecule organic solar cells with high efficiency over 11%. *J. Mater. Chem. A* **7**, 3682–3690 (2019).
179. Yang, L. et al. Modulating molecular orientation enables efficient nonfullerene small-molecule organic solar cells. *Chem. Mater.* **30**, 2129–2134 (2018).
180. Xu, C. et al. Recent progress in all-small-molecule organic photovoltaics. *J. Mater. Chem. A* **10**, 6291–6329 (2022).
181. Ye, W. et al. Nonfullerene all-small-molecule organic solar cells: prospect and limitation. *Sol. RRL* **4**, 2000258 (2020).

182. Tang, H. et al. Benzodithiophene-based small-molecule donors for next-generation all-small-molecule organic photovoltaics. *Matter* **3**, 1403–1432 (2020).
183. Chang, Y. et al. Constructing high-performance all-small-molecule ternary solar cells with the same third component but different mechanisms for fullerene and non-fullerene systems. *Adv. Energy Mater.* **9**, 1900190 (2019).
184. Shan, T. et al. Spatially orthogonal 2D sidechains optimize morphology in all-small-molecule organic solar cells. *Adv. Funct. Mater.* **31**, 2100750 (2021).
185. Ge, J. et al. Asymmetric substitution of end-groups triggers 16.34% efficiency for all-small-molecule organic solar cells. *Adv. Mater.* **34**, 2202752 (2022).
186. Ge, J. et al. Solvent annealing enables 15.39% efficiency all-small-molecule solar cells through improved molecule interconnection and reduced non-radiative loss. *Adv. Energy Mater.* **11**, 2100800 (2021).
187. Jiang, M. et al. Rational compatibility in a ternary matrix enables all-small-molecule organic solar cells with over 16% efficiency. *Energy Environ. Sci.* **14**, 3945–3953 (2021).
188. Liu, Y. et al. High-performance solar cells using a solution-processed small molecule containing benzodithiophene unit. *Adv. Mater.* **23**, 5387–5391 (2011).
189. Zhou, J. et al. Small molecules based on benzo[1,2-b:4,5-b']dithiophene unit for high-performance solution-processed organic solar cells. *J. Am. Chem. Soc.* **134**, 16345–16351 (2012).
190. Kan, B. et al. Solution-processed organic solar cells based on dialkylthiol-substituted benzodithiophene unit with efficiency near 10%. *J. Am. Chem. Soc.* **136**, 15529–15532 (2014).
191. Sun, K. et al. A molecular nematic liquid crystalline material for high-performance organic photovoltaics. *Nat. Commun.* **6**, 6013 (2015).
192. Tang, H. et al. Donor derivative incorporation: an effective strategy toward high performance all-small-molecule ternary organic solar cells. *Adv. Sci.* **6**, 1901613 (2019).
193. Cui, Y. et al. Over 16% efficiency organic photovoltaic cells enabled by a chlorinated acceptor with increased open-circuit voltages. *Nat. Commun.* **10**, 2515 (2019).
194. Jiang, M. et al. Two-pronged effect of warm solution and solvent–vapor annealing for efficient and stable all-small-molecule organic solar cells. *ACS Energy Lett.* **6**, 2898–2906 (2021).
195. Li, Z. et al. Over 17% efficiency all-small-molecule organic solar cells based on an organic molecular donor employing a 2D side chain symmetry breaking strategy. *Energy Environ. Sci.* **15**, 4338–4348 (2022).
196. Li, H. et al. Liquid-crystalline small molecules for nonfullerene solar cells with high fill factors and power conversion efficiencies. *Adv. Energy Mater.* **9**, 1803175 (2019).
197. Gao, K. et al. Over 12% efficiency nonfullerene all-small-molecule organic solar cells with sequentially evolved multilength scale morphologies. *Adv. Mater.* **31**, 1807842 (2019).
198. Sun, R. et al. High-efficiency all-small-molecule organic solar cells based on an organic molecule donor with an asymmetric thieno[2,3-f] benzofuran unit. *Sci. China Chem.* **63**, 1246–1255 (2020).
199. Wang, X. et al. Over 15% efficiency all-small-molecule organic solar cells enabled by a C-shaped small molecule donor with tailorable asymmetric backbone. *Nano Energy* **81**, 105612 (2021).
200. Hu, D. et al. A volatile solid additive enables oligothiophene all-small-molecule organic solar cells with excellent commercial viability. *Adv. Funct. Mater.* **33**, 2211873 (2023).
201. Nian, L. et al. Approaching 16% efficiency in all-small-molecule organic solar cells based on ternary strategy with a highly crystalline acceptor. *Joule* **4**, 2223–2236 (2020).
202. Sun, Y. et al. Rational control of sequential morphology evolution and vertical distribution toward 17.18% efficiency all-small-molecule organic solar cells. *Joule* **6**, 2835–2848 (2022).
203. Yang, L. et al. Parallel-like bulk heterojunction polymer solar cells. *J. Am. Chem. Soc.* **134**, 5432–5435 (2012).
204. Khlyabich, P. P. et al. Compositional dependence of the open-circuit voltage in ternary blend bulk heterojunction solar cells based on two donor polymers. *J. Am. Chem. Soc.* **134**, 9074–9077 (2012).
205. Khlyabich, P. P. et al. Efficient ternary blend bulk heterojunction solar cells with tunable open-circuit voltage. *J. Am. Chem. Soc.* **133**, 14534–14537 (2011).
206. Street, R. A. et al. Origin of the tunable open-circuit voltage in ternary blend bulk heterojunction organic solar cells. *J. Am. Chem. Soc.* **135**, 986–989 (2013).
207. Liu, T. et al. Use of two structurally similar small molecular acceptors enabling ternary organic solar cells with high efficiencies and fill factors. *Energy Environ. Sci.* **11**, 3275–3282 (2018).
208. Hultmark, S. et al. Suppressing co-crystallization of halogenated non-fullerene acceptors for thermally stable ternary solar cells. *Adv. Funct. Mater.* **30**, 2005462 (2020).
209. Jung, S. et al. Effect of third component on efficiency and stability in ternary organic solar cells: more than a simple superposition. *Sol. RRL* **6**, 2100819 (2022).
210. Xu, X. et al. Ternary blend organic solar cells: understanding the morphology from recent progress. *Adv. Mater.* **34**, 2107476 (2022).
211. Fan, B. et al. Formation of vitrified solid solution enables simultaneously efficient and stable organic solar cells. *ACS Energy Lett.* **6**, 3522–3529 (2021).
212. Zhang, G. et al. Nonfullerene acceptor molecules for bulk heterojunction organic solar cells. *Chem. Rev.* **118**, 3447–3507 (2018).
213. Zhu, Y. et al. Rational strategy to stabilize an unstable high-efficiency binary nonfullerene organic solar cells with a third component. *Adv. Energy Mater.* **9**, 1900376 (2019).
214. Xie, Y. et al. Morphology control enables efficient ternary organic solar cells. *Adv. Mater.* **30**, 1803045 (2018).
215. Zhang, H. et al. Improved domain size and purity enables efficient all-small-molecule ternary solar cells. *Adv. Mater.* **29**, 1703777 (2017).
216. Li, N. et al. Abnormal strong burn-in degradation of highly efficient polymer solar cells caused by spinodal donor-acceptor demixing. *Nat. Commun.* **8**, 14541 (2017).
217. He, Y. et al. Industrial viability of single-component organic solar cells. *Joule* **6**, 1160–1171 (2022).
218. Liang, S. et al. Double-cable conjugated polymers with pendant rylene diimides for single-component organic solar cells. *Acc. Chem. Res.* **54**, 2227–2237 (2021).
219. He, Y. et al. Evidencing excellent thermal- and photostability for single-component organic solar cells with inherently built-in microstructure. *Adv. Energy Mater.* **9**, 1900409 (2019).
220. Lai, W. et al. Diketopyrrolopyrrole-based conjugated polymers with perylene bisimide side chains for single-component organic solar cells. *Chem. Mater.* **29**, 7073–7077 (2017).
221. Yang, X. et al. Over 13% efficient single-component organic solar cells enabled by adjusting the conjugated-length of intermediate PBDB-T block. *Adv. Funct. Mater.* **33**, 2208412 (2023).
222. Liu, S. et al. Printable and large-area organic solar cells enabled by a ternary pseudo-planar heterojunction strategy. *Adv. Funct. Mater.* **30**, 2003223 (2020).
223. Sun, R. et al. A multi-objective optimization-based layer-by-layer blade-coating approach for organic solar cells: rational control of vertical stratification for high performance. *Energy Environ. Sci.* **12**, 3118–3132 (2019).
224. Sun, R. et al. A layer-by-layer architecture for printable organic solar cells overcoming the scaling lag of module efficiency. *Joule* **4**, 407–419 (2020).
225. Jee, M. H. et al. Recent advances in nonfullerene acceptor-based layer-by-layer organic solar cells using a solution process. *Adv. Sci.* **9**, 2201876 (2022).
226. Guo, S. et al. Toward high-performance organic photovoltaics: the new cooperation of sequential solution-processing and promising non-fullerene acceptors. *Mater. Horiz.* **9**, 2097–2108 (2022).
227. Xu, X. et al. Sequential deposition of multicomponent bulk heterojunctions increases efficiency of organic solar cells. *Adv. Mater.* **35**, 2208997 (2023).
228. Chen, T. et al. Compromising charge generation and recombination of organic photovoltaics with mixed diluents strategy for certified 19.4% efficiency. *Adv. Mater.* **35**, e2300400 (2023).
229. Yang, W. et al. Balancing the efficiency, stability, and cost potential for organic solar cells via a new figure of merit. *Joule* **5**, 1209–1230 (2021).
230. Li, N. et al. Analyzing the efficiency, stability and cost potential for fullerene-free organic photovoltaics in one figure of merit. *Energy Environ. Sci.* **11**, 1355–1361 (2018).
231. Lee, J.-W. et al. Linker engineering of dimerized small molecule acceptors for highly efficient and stable organic solar cells. *ACS Energy Lett.* **8**, 1344–1353 (2023).
232. Sun, C. et al. Dimerized small-molecule acceptors enable efficient and stable organic solar cells. *Joule* **7**, 416–430 (2023).
233. Zhang, L. et al. 'N-π-N' type oligomeric acceptor achieves an OPV efficiency of 18.19% with low energy loss and excellent stability. *Adv. Sci.* **9**, 2202513 (2022).
234. Li, S. et al. Tethered small-molecule acceptors simultaneously enhance the efficiency and stability of polymer solar cells. *Adv. Mater.* **35**, 2206563 (2023).
235. Langner, S. et al. Beyond ternary OPV: high-throughput experimentation and self-driving laboratories optimize multicomponent systems. *Adv. Mater.* **32**, 1907801 (2020).
236. Du, X. et al. Elucidating the full potential of OPV materials utilizing a high-throughput robot-based platform and machine learning. *Joule* **5**, 495–506 (2021).
237. MacLeod, B. P. et al. Self-driving laboratory for accelerated discovery of thin-film materials. *Sci. Adv.* **6**, eaaz8867 (2020).
238. Sun, R. et al. 18.2%-Efficient ternary all-polymer organic solar cells with improved stability enabled by a chlorinated guest polymer acceptor. *Joule* **7**, 221–237 (2023).
239. Ma, R. et al. Unveiling the morphological and physical mechanism of burn-in loss alleviation by ternary matrix toward stable and efficient all-polymer solar cells. *Adv. Mater.* **35**, e2212275 (2023).
240. Hu, D. et al. 15.34% Efficiency all-small-molecule organic solar cells with an improved fill factor enabled by a fullerene additive. *Energy Environ. Sci.* **13**, 2134–2141 (2020).
241. Piradi, V. et al. Panchromatic ternary organic solar cells with porphyrin dimers and absorption-complementary benzodithiophene-based small molecules. *ACS Appl. Mater. Interfaces* **11**, 6283–6291 (2019).
242. Zhang, Z. et al. Polymerized small-molecule acceptor as an interface modulator to increase the performance of all-small-molecule solar cells. *Adv. Energy Mater.* **12**, 2102394 (2022).
243. Jin, K. et al. 18.69% PCE from organic solar cells. *J. Semiconduct.* **42**, 060502 (2021).
244. Yu, X. et al. Ternary organic solar cells with enhanced charge transfer and stability combining the advantages of polymer acceptors and fullerene acceptors. *Org. Electron.* **104**, 106471 (2022).

Acknowledgements

H. Yan acknowledges support from a Tencent Xplorer Prize.

Author contributions

J.Y., G.Z. and H. Yu researched data for the paper. All authors contributed substantially to discussion of the content, wrote the paper and reviewed and/or edited the paper before submission.

Competing interests

The authors declare no competing interests.

Additional information

Supplementary information The online version contains supplementary material available at https://doi.org/10.1038/s41578-023-00618-1.

Peer review information *Nature Reviews Materials* thanks Xian-Kai Chen and the other, anonymous, reviewer(s) for their contribution to the peer review of this work.

Publisher's note Springer Nature remains neutral with regard to jurisdictional claims in published maps and institutional affiliations.